Journal of Structural Geology 30 (2008) 1332–1347

Contents lists available at ScienceDirect

Journal of Structural Geology

journal homepage: www.elsevier.com/locate/jsg

Evolution of quartz microstructure and *c*-axis crystallographic preferred orientation within ductilely deformed granitoids (Arolla unit, Western Alps)

Luca Menegon [a,*], Giorgio Pennacchioni [a], Renee Heilbronner [b], Lidia Pittarello [a]

[a] Dipartimento di Geoscienze, Università di Padova, Via Giotto 1, 35137 Padova, Italy
[b] Geological Institute, Department of Environmental Sciences, University of Basel, Bernoullistrasse 32, CH-4056 Basel, Switzerland

ARTICLE INFO

Article history:
Received 30 November 2007
Received in revised form 19 June 2008
Accepted 4 July 2008
Available online 6 August 2008

Keywords:
Quartz *c*-axis CPO
Quartz microstructure
Optical orientation imaging
Ductile deformation of granitoids
Deformation partitioning

ABSTRACT

We have studied quartz microstructures and the *c*-axis crystallographic preferred orientations (CPOs) in four granitoid samples representative of increasing ductile shear deformation, from a weakly deformed granitoid (stage 1) to a mylonitic granitoid (stage 4). The quartz *c*-axis CPO measured in the mylonitic granitoid has been compared with the one observed in a fully recrystallized quartz mylonite from the same area. All the samples belong to the Austroalpine Arolla unit (Western Alps) and were deformed at greenschist facies conditions. The quartz *c*-axis CPO was analyzed using a U-stage and the optical orientation imaging technique. The magmatic plagioclase, forming more than 50% of the volume of the granitoid, is extensively replaced by a mica-rich aggregate even in weakly deformed samples of stage 1. These aggregates flow to form an interconnected weak matrix with increasing deformation, wrapping relatively less strained quartz grains that undergo dominantly coaxial strain. Recrystallization of quartz ranges from less than 1% in the weakly deformed granitoid to up to 85% in the mylonitic granitoid, with average grain strain of 41% and 64%, respectively. With increasing strain and recrystallization, quartz grains in the granitoids show a sequence of transient microstructures and CPOs. Crystal plastic deformation is initially accomplished by dislocation glide with limited recovery, and at 50% grain strain it results in a CPO consistent with dominantly basal ⟨*a*⟩ slip. At 60% grain strain, recrystallization is preferentially localized along shear bands, which appear to develop along former intragranular cracks, and the recrystallized grains develop a strong *c*-axis CPO with maxima orthogonal to the shear band boundaries and independent of the host grain orientation. Within the granitoid mylonite, at an average quartz grain strain of 64%, recrystallization is extensive and the *c*-axis CPO of new grains displays maxima overlapping the host *c*-axis orientation and, therefore, unrelated to the bulk sense of shear. The host-controlled CPO is inferred to reflect pervasive recrystallization by progressive subgrain rotation. The switch from 'shear band-control' to 'host-control' on *c*-axis CPO occurred between 40% and 70% of recrystallization. In the quartz mylonite, the quartz *c*-axis CPO develops an asymmetric single girdle consistent with the bulk sense of shear and the synkinematic greenschist facies conditions. This study indicates that the CPO evolution of quartz may significantly differ in cases of polymineralic vs. monomineralic rocks under the same deformation conditions, if quartz in the polymineralic rock behaves as a 'strong' phase.

1. Introduction

The microstructures and *c*-axis preferred orientations (CPOs) of quartz in naturally deformed rocks are widely considered as gauges for different deformation and physical parameters, such as strain geometry (Schmid and Casey, 1986; Law, 1990), sense of shear (Simpson and Schmid, 1983), and temperature of deformation (Stipp et al., 2002). Most of the current knowledge of quartz *c*-axis CPO arises from the study of experimentally (e.g., Hirth and Tullis, 1992; Gleason et al., 1993; Heilbronner and Tullis, 2002, 2006) and naturally (e.g., Mancktelow, 1987; Pauli et al., 1996; Dunlap et al., 1997; Stöckhert et al., 1999; Stipp et al., 2002) deformed pure quartz rocks, as well as from computer simulations of CPO development within monomineralic aggregates (e.g., Lister and Hobbs, 1980). However, the continental lithosphere mostly consists of polymineralic aggregates, and a prominent question in microstructural studies is whether the quartz CPOs commonly observed in pure quartz aggregates as a result of crystal plastic deformation develop in polyphase rocks as well (e.g., granitoids) under the same metamorphic and deformation conditions (e.g., Dell'Angelo and Tullis, 1986).

* Corresponding author. Tel.: +39 049 8273941; fax: +39 049 8272070.
E-mail address: luca.menegon@unipd.it (L. Menegon).

0191-8141/$ – see front matter © 2008 Elsevier Ltd. All rights reserved.
doi:10.1016/j.jsg.2008.07.007

The rheological behaviour of quartzo-feldspathic aggregates is still poorly understood but it is certainly determined by a complex feedback between relative mineral amounts, phase arrangement, phase strength contrast and degree of mineral reaction (e.g., Dell'Angelo and Tullis, 1996; Passchier and Trouw, 1996; Holyoke and Tullis, 2006).

In many granitoid mylonites deformed under greenschist facies conditions, quartz is reported as a weak mineral and occurs as ribbons or as elongated aggregates of recrystallized new grains. Quartz aggregates outline the foliation together with mica aggregates, whereas K-feldspar commonly occurs as porphyroclasts and undergoes fracturing and fragmentation (e.g., Simpson, 1985; Gapais, 1989; Fitz Gerald and Stünitz, 1993; Passchier and Trouw, 1996; Hippertt, 1998; Vernon, 2004). In these cases, quartz commonly forms an interconnected network of weak layers (Handy, 1990) that deform by dominantly simple shear along the foliation, as suggested by the monoclinic symmetry of several microstructural indicators including the CPO. Under these circumstances, quartz is assumed to control the rheology of the bulk rock and quartz grain size piezometer can be used to infer the rock flow strength.

The development of quartz *c*-axis CPOs within a bimineralic quartz–feldspar aggregate was investigated by Dell'Angelo and Tullis (1986) who performed axial compression experiments on aplite and pure quartzite under conditions where quartz deformed predominantly by basal slip with very minor dynamic recrystallization. Aplite and quartzite were deformed to the same amount of finite strain and at 800 and 900 °C. Although aplite started out with a stress-supporting framework of feldspars, in the higher T experiments (900 °C) quartz became increasingly connected above ~40% strain and behaved as the weak phase dominating the flow stress of the rock. Quartz grains developed the same *c*-axis CPO pattern as that in a pure quartzite deformed at the same conditions and at approximately the same quartz grain strains. However, main limitations in extrapolating these observations to natural quartzo-feldspathic aggregates deformed at greenschist facies conditions are the very minor recrystallization of quartz in the experiments and the very low strains possibly in axial compression experiments.

In addition, under greenschist facies conditions, the plagioclase in deformed granitoids is often extensively altered to fine-grained aggregates of white mica, albite and epidote (Fitz Gerald and Stünitz, 1993; Tourigny and Tremblay, 1997; Hippertt, 1998; Gueydan et al., 2003; Park et al., 2006). This replacement has a major weakening effect on the plagioclase and on the bulk rock due to the combined effect of the presence of mica, which is a weak phase (Shea and Kronenberg, 1993), and the grain size reduction which is in general regarded as a softening mechanism because of the onset of grain size sensitive creep (Fitz Gerald and Stünitz, 1993; Stünitz and Fitz Gerald, 1993; Stünitz and Tullis, 2001; Gueydan et al., 2003; Holyoke and Tullis, 2006). Under these circumstances the rock rheology is strongly influenced by the flow of the plagioclase-replacing aggregates that are weaker than quartz and behave as the stress-supporting framework of the rock. In such a case, due to deformation partitioning (e.g., Lister and Williams, 1983; Bell, 1985; Goodwin and Tikoff, 2002) quartz may behave as a relatively hard mineral and undergo a dominantly coaxial deformation in a regime of non-coaxial bulk deformation with the plagioclase-derived matrix accommodating a dominantly simple shear deformation.

In the present paper we describe the microstructure and *c*-axis CPO of quartz during progressive shear deformation of granitoids. The studied samples belong to the Austroalpine Arolla unit (Western Italian Alps) and the deformation occurred at greenschist facies under fluid-rich conditions. During the incipient stage of the deformation, plagioclase reacted to a very soft matrix, leaving the quartz as a relatively 'hard phase' throughout the whole deformation history. The aim of the study is to document the progressive development of a CPO of both old- and dynamically recrystallized quartz grains within a polyphase aggregate where quartz behaves as a strong phase and does not represent the stress-supporting mineral of the bulk rock. It will be shown that the evolution of quartz microstructures and *c*-axis CPOs includes transient stages that depend both on the amount of strain and on the orientation of the original quartz grain. This evolution may be rather common in greenschist facies granitoid mylonites.

We also report a comparison between the quartz CPO in the granitoids and in a mylonitic quartz vein belonging to the same tectonic unit and deformed at the same metamorphic conditions during the Alpine orogeny. We wanted to determine whether or not the recrystallized quartz *c*-axis CPO patterns in granitoids are systematically similar to any standard pattern commonly observed in quartz mylonites. This study demonstrates that the CPO patterns depend greatly on the different strain paths experienced by quartz within monomineralic vs. polymineralic rocks.

2. Geological setting and sample description

The Arolla unit belongs to the composite Austroalpine Dent Blanche nappe of the North-Western Alps, Italy (Dal Piaz et al., 1972; Pennacchioni and Guermani, 1993) (Fig. 1a). In this unit, late Paleozoic granitoids were extensively converted to greenschist facies tectonites and mylonites (Arolla gneisses and mylonites: Pennacchioni and Guermani, 1993) during the Alpine orogeny, but escaped strong Alpine reworking in metre to 100 m scale domains. The best examples of these Alpine low-strain domains are located within the Comba di Crete Sèche, on the western side of the Valpelline Valley (Fig. 1b). Here the primary intrusive contact between pre-Alpine high-grade paragneisses and the granitoids is preserved. The Alpine greenschist facies mylonitic foliation is moderately to steeply NW-dipping and the stretching lineation, associated with a top-to-the-NW sense of tectonic transport, trends NW–SE (see orientation data in Fig. 1b, and Pennacchioni and Guermani, 1993). In the field, the transition from weakly deformed to mylonitic rocks usually occurs over distances of several metres. The low-strain pods are bounded by fine-grained orthogneisses and mylonitic granitoids, in an irregular alternation of variably strained rocks.

We have grouped an overall selection of eight granitoid samples into four stages of increasing intensity of ductile deformation. The samples include, from the least to the most intensely deformed: two weakly deformed granitoids (samples M44G and SPA2: stage 1 of deformation), two moderately deformed granitoids (samples M1G and M2G: stage 2), and four mylonites (samples M3G and M4G: stage 3; M30G1 and M30G2: stage 4) (Fig. 2). A millimetre-thick mylonitic quartz vein (sample DBL2090) transposed along the foliation of samples M30G was also investigated to compare the quartz microstructure and the CPO developing in the polymineralic granitoid and in a monomineralic rock.

The mineral composition of the granitoid protolith, determined in samples M44G and SPA2, includes plagioclase (54% volume), quartz (31%), biotite (12%), K-feldspar (2%), hornblende (1%) and accessory apatite, allanite, epidote and zircon. The metamorphic assemblage synkinematic to the Alpine deformation consists of quartz + albite + chlorite + epidote + muscovite + actinolite + titanite ± stilpnomelane, indicating greenschist facies conditions. Mylonitization of granitoids occurred under fluid-rich conditions, as indicated by the synkinematic formation of muscovite and epidote (derived from plagioclase breakdown) and chlorite (derived from biotite breakdown).

The relative intensity of the Alpine strain within each sample was established on the basis of: (i) the degree of development of the prominent Alpine foliation as estimated in the hand-specimen and in thin section (Fig. 2), (ii) the degree of replacement of the

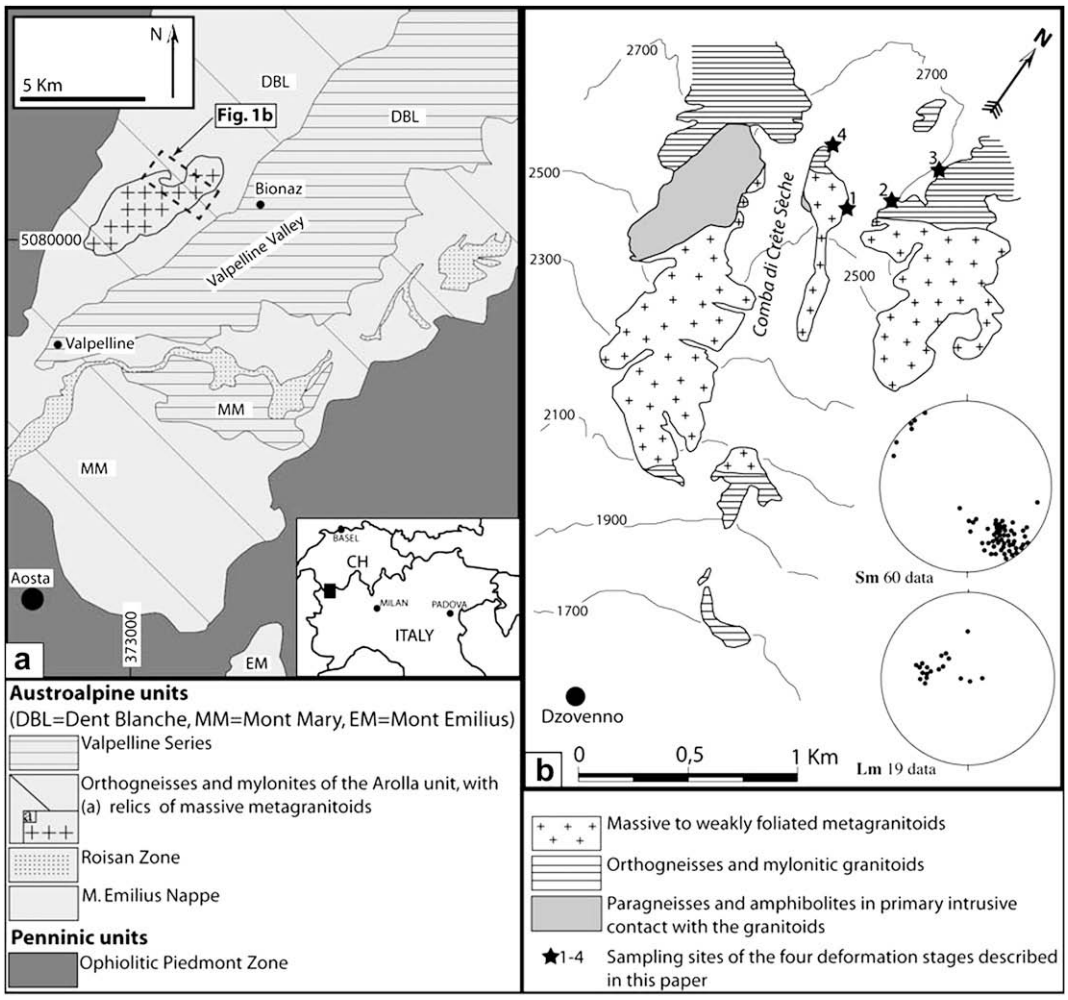

Fig. 1. (a) Tectonic sketch of the Dent Blanche nappe and of the adjoining units (Western Alps) redrawn and modified from Pennacchioni and Guermani (1993). (b) Simplified geological map of the sampling site, located in the kilometre-scale low-strain domain of the Comba di Crete Sèche. Redrawn and modified from Pennacchioni and Guermani (1993). Pole figures of the Alpine foliation (Sm) and stretching lineation (Lm) in the sampling area are shown.

magmatic minerals (K-feldspar, biotite and hornblende) by Alpine synkinematic metamorphic minerals (albite, chlorite and actinolite), (iii) the degree of recrystallization of quartz (Fig. 3), and (iv) the average grain strain of quartz estimated from the average aspect ratio of the gains.

The fine-grained metamorphic aggregates developed at the expense of the magmatic minerals behaved as a relatively weak matrix. As a consequence, increasing metamorphic replacement led to increasing partitioning of the deformation into the matrix.

A large part of the deforming matrix is composed of fine-grained albite + epidote + sericite aggregates derived from the fluid-assisted replacement of magmatic plagioclase. This metamorphic reaction is extensive even in stage 1, where the replacement aggregate develops from intragranular fractures towards the interior of the grain, along cleavage planes and mimetic on the primary twinning. The replacement reaction was promoted by cataclastic deformation of primary plagioclase, and the reaction products flowed in stage 2 samples to interconnected layers of weak matrix forming the stress-supporting framework of the strained granitoids.

Perthitic K-feldspar behaved brittlely during the first stages of deformation. It shows diffuse fractures along the cleavage planes decorated with neocrystallizated albite aggregates (e.g., see Fitz Gerald and Stünitz, 1993). Within mylonitic stages 3 and 4 of deformation, the original K-feldspar porphyroclasts are totally replaced by a fine-grained aggregate of albite grains (about 10 μm average diameter), which are variably elongated into the foliation.

3. Methods of study

The optical microstructure and the quartz *c*-axis CPO have been investigated in several thin sections of each sample cut orthogonal to the foliation and parallel to the stretching lineations. We produced line drawings of different thin sections and performed digital image analysis to determine (1) the spatial arrangement and the best-fit ellipse of quartz porphyroclasts, (2) the proportions of recrystallized grains and relict magmatic quartz, and (3) the modal composition of the starting granitoid. For each porphyroclast, we determined the aspect ratios (a/b, i.e., long/short axis) of the best-fit ellipse and the diameter of the circle with an area equivalent to that of the ellipse. From the best-fit ellipse we derived the quartz grain strain, in the form of (1) the maximum extension (i.e., as the elongation along the *X*-direction of the diameter of the equivalent circle), and (2) the longitudinal strain, assuming constant volume and initial equant shape (Table 1). The best-fit ellipses of the quartz grains were also employed for a quantitative estimate of the intensity of the fabric of the deformed granitoids by the use of the mean vector strength ($\overline{a}$) defined by the equation (Cladouhos, 1999):

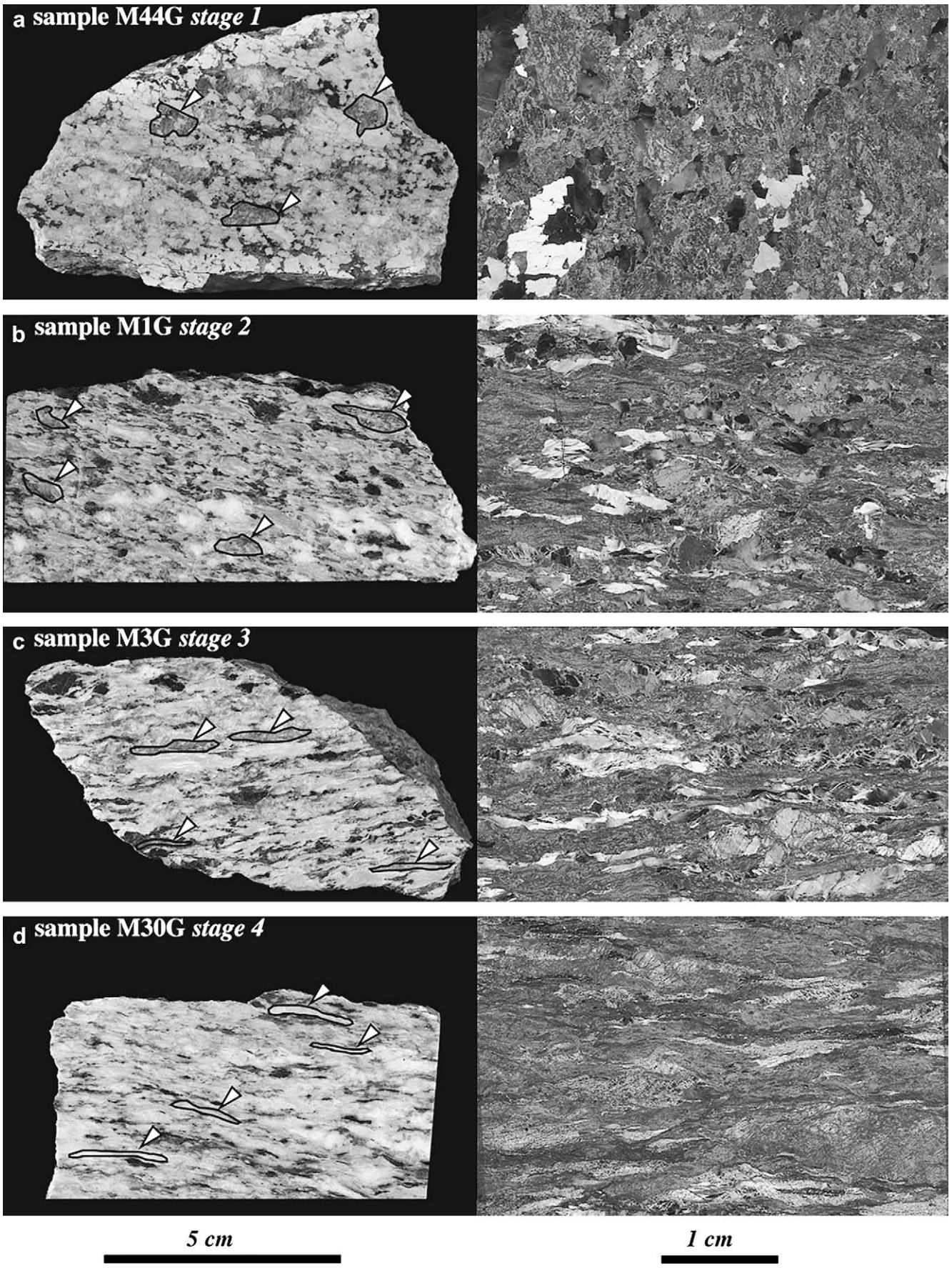

Fig. 2. Hand samples and thin sections (crossed polarizer) of the selected granitoid samples: (a) M44G (stage 1: weakly deformed); (b) M1G (stage 2: moderately deformed); (c) M3G (stage 3: mylonitic); (d) M30G (stage 4: mylonitic). Some quartz grains in the hand samples photos are outlined and pointed out by arrows.

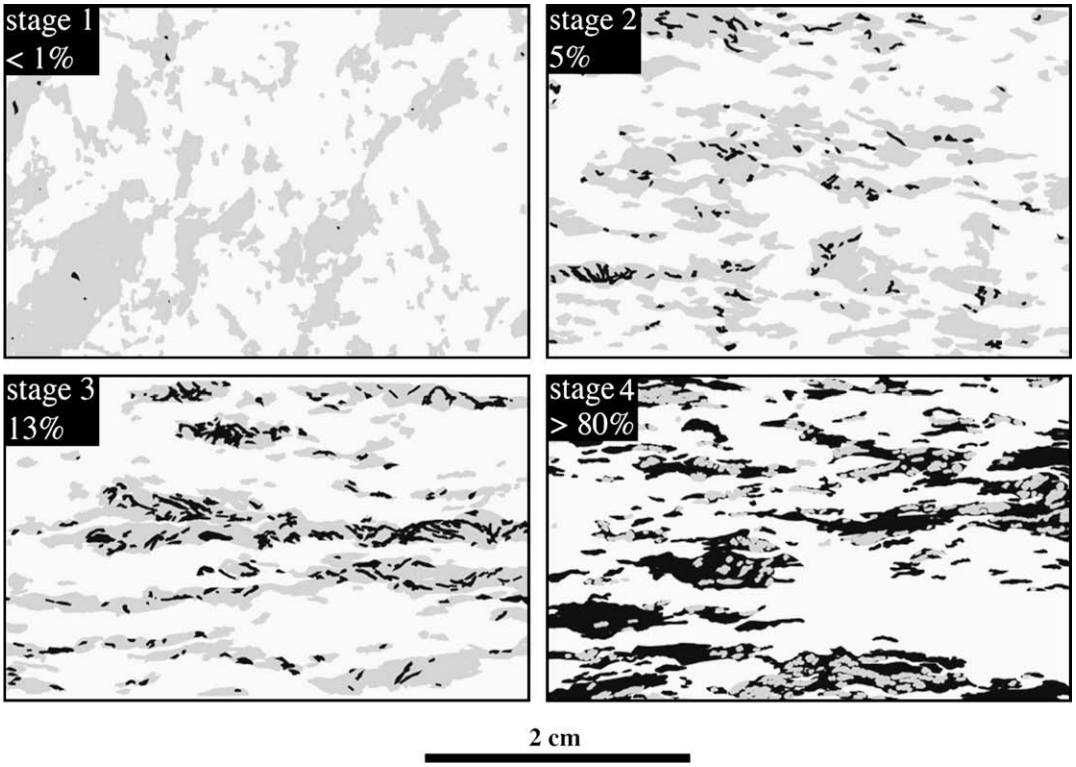

Fig. 3. Spatial distribution of quartz domains within thin sections of the samples shown in Fig. 2. Light grey = magmatic quartz; black = recrystallized grains, volume percentage is indicated in upper left corner.

$$\overline{a} = \frac{1}{N}\left\{\left(\sum \sin 2\theta_i\right)^2 + \left(\sum \cos 2\theta_i\right)^2\right\}^{1/2} \quad (1)$$

where N is the number of measured quartz grains and θ_i is the angle between the quartz porphyroclast long axis and the foliation, measured in an anticlockwise sense. The magnitude of the vector mean strength $\overline{a}$ varies from zero for a perfectly uniform distribution to one for a population of parallel lines. Low values of $\overline{a}$ are expected in weakly deformed granitoids where relatively low aspect ratio porphyroclasts are not well aligned with the incipient foliation, whereas values of $\overline{a}$ close to one are typical of a mature mylonite where porphyroclasts have been rotated and stretched parallel to the foliation.

On all microstructural images and pole figures, the reference axes are set as follows: the *Y*-direction is normal to the image plane pointing downwards, the *X*-direction (parallel to the stretching lineation direction) is horizontal, and the *Z*-direction (corresponding to the foliation normal) is vertical, pointing upwards. The bulk sense of shear is represented as dextral in both the deformed granitoids and quartz vein, and corresponds to the top-to-NW sense of tectonic transport determined in the Arolla mylonites (Pennacchioni and Guermani, 1993). Crystallographic orientations are plotted in the upper hemisphere of the Schmidt projection, with the following conventions: the azimuth of the *c*-axes ranges from 0° to 180° and is measured clockwise from the positive *Z*-direction, and the inclination of the *c*-axes ranges from 0° to 180° and is measured from the negative to the positive *Y*-direction (inclination of *X*- and *Z*-directions is 90°).

Measurements of the *c*-axis CPO of quartz have been carried out both on old and recrystallized grains. Depending on the grain size, the quartz *c*-axis orientations were measured by U-stage or computer-integrated polarization microscopy (CIP: Panozzo Heilbronner and Pauli, 1993). While the U-stage measurements usually record one *c*-axis orientation per grain, the CIP analysis yields the *c*-axis orientation at each pixel of the image. Two-dimensional colour look-up tables (CLUTs) represent the *c*-axis orientation in *c-axis orientation images* (COIs), similar to the AVA images (i.e., "Achsen-Verteilungs-Analyse": analysis of distribution of axes) introduced by Sander (1950). The CIP method is a method of orientation imaging allowing simultaneous visualization of microstructure and texture. Using CIP, area-weighted pole figures of the entire COIs or of selected areas can be derived. Further details of the method are

Table 1
Amount of recrystallization, average shape and strain, and intensity of SPO of quartz porphyroclasts in the four deformation stages

Stage of deformation	Amount of recrystallization[a] (%)	Measured porphyroclasts	Aspect ratio R (a/b)	Quartz extension e_x[b]	Quartz grain strain ε (%)[c]	Vector mean strength $\bar{a}$[d]
1	<1	193	2.2	0.4	41	0.24
2	5	186	2.8	0.6	50	0.64
3	10	73	4.1	1.0	61	0.90
4	>80	192	4.6	1.1	64	0.90

[a] Expressed as volume fraction of recrystallized grains with respect to the total quartz.
[b] Maximum extension values are expressed by the elongation of the diameter of the equivalent circle along the *X*-direction.
[c] Grain longitudinal strain values derived from the aspect ratio R of the best-fit ellipse: $\varepsilon(\%) = 100\,(1 - R^{-2/3})$, see Den Brok (1992) and Dell'Angelo and Tullis (1996).
[d] Vector mean strength $\overline{a} = \frac{1}{N}\{(\sum \sin 2\theta_i)^2 + (\sum \cos 2\theta_i)^2\}^{1/2}$, where N is the number of measured porphyroclasts and θ_i is the angle between the porphyroclast long axis and the foliation, measured in an anticlockwise sense. Only porphyroclasts with $R > 1.3$ have been measured, following the procedure of Cladouhos (1999).

given in Panozzo Heilbronner and Pauli (1993) and Heilbronner (2000).

Thin sections of stage 1 and 2 samples were analyzed with a Leitz U-stage on a Zeiss microscope. In the case of strong undulatory or banded extinction, the average orientation representative of the single grain was chosen.

Thin sections of stage 3 and 4 samples and of the mylonitic quartz vein were analyzed with a Zeiss Axioplan microscope with an objective of 2.5× magnification. The input images for the CIP method were acquired with a Zeiss AxioCam MRm digital camera. After preprocessing the azimuth and inclination images, the COIs and the pole figure matrices were calculated by the CIP software (Panozzo Heilbronner and Pauli, 1993). Portions of the images that were not occupied by quartz were masked. The so-called spectrum CLUT was chosen to visualize the CPO. It represents the *Z*-direction in blue, the *X*-direction in yellow and the *Y*-direction in white. In one case we used a separate CLUT highlighting specific orientation domains.

4. Results

4.1. Spatial arrangement of quartz and grain strain

The spatial arrangement of quartz in the four deformation stages has been evaluated by inspection of thin section line drawings (Fig. 3). The bitmaps demonstrate that the average flattening and elongation of quartz porphyroclasts increases progressively from stage 1 to stage 4, but without forming highly interconnected domains. In all samples quartz basically forms dispersed grains in the plagioclase-derived matrix that takes up most of the ductile strain. Average aspect ratio of porphyroclasts increases from 2.2 in stage 1 to 4.6 in stage 4, corresponding to maximum extension values ranging from 0.4 to 1.1 and to longitudinal strain ranging from 41% to 64%, respectively (Table 1). This increase in the average grain strain is associated with a progressively stronger preferred shape orientation of quartz porphyroclasts parallel to the foliation as indicated by the increase of the vector mean strength for porphyroclasts from 0.24 (stage 1) to 0.9 (stages 3–4).

4.2. Quartz microstructure

4.2.1. Deformed granitoids

In samples M44G and SPA2 (stage 1 of deformation; 41% average grain strain), the magmatic quartz grains show an equant to slightly elongated shape defining a weak shape preferred orientation (SPO) parallel to the incipient foliation. The average ellipticity of quartz grains is 2.2 and the intensity of the SPO of quartz grains measured as mean vector strength is 0.24 (Fig. 3; Table 1). Deformation microstructures of quartz include undulatory to patchy extinction, deformation lamellae and minor deformation bands and subgrains (Fig. 4a). Quartz–quartz grain boundaries show small-scale bulges, locally associated with the new grains (less than 1% volume of the total quartz) <20 μm in diameter (Fig. 4b). Bulges are also present along fractures and grain boundaries irrespective of their orientation with respect to foliation.

In samples M1G and M2G (stage 2 of deformation; 50% average grain strain), quartz shows a clear SPO subparallel to the foliation (mean vector strength: 0.64) and includes ~5% volume of recrystallized grains (Fig. 3; Table 1). Quartz grains include healed fractures outlined by fluid inclusion trails (mostly oriented at 60°–90° to the foliation), narrow (less than 50 μm thick) conjugate shear bands having the same orientation as, and often coinciding with, the healed fractures (Fig. 4c and d), and wide (up to 100 μm thick) deformation bands and kink bands, mainly oriented at about 20°–40° to the foliation (Fig. 4e). In some places, the shear bands are recrystallized to layers of 1–2 new grains in thickness (20 μm–50 μm average grain size). Small bulges are developed along both grain boundaries and deformation band boundaries irrespective of their orientation. The host quartz grains commonly show wavy and undulatory extinction, making a transition to polygonized domains formed by equant, blocky subgrains (10 μm–30 μm). The subgrains are frequently arranged in subparallel and/or conjugate layers inclined at ~45° to the *Z*-direction (Fig. 5f). Progressive misorientation from subgrains to new recrystallized grains (20 μm–50 μm) can be locally observed at the periphery of quartz porphyroclasts or towards the deformation band boundaries.

In samples M3G and M4G (stage 3 of deformation; 60% average grain strain), quartz porphyroclasts with an average aspect ratio of 4.1 are well aligned in the foliation ($\bar{a} = 0.9$) (Fig. 3; Table 1). In these samples new quartz grains form ~13% of the total quartz volume and up to 40% in some porphyroclasts (see Fig. 3). The new grains range from 20 μm to 100 μm in diameter and are arranged along recrystallization bands inclined at 30°–45° to the foliation. These bands occur both as one set of subparallel structures and as two sets of conjugate bands intersecting at an angle of ~100°–120° (Fig. 5a). The conjugate sets are most clearly developed in porphyroclasts with their *c*-axes oriented subparallel to the *Z*-direction. The recrystallized bands are one to several grains wide and the new grains have an average diameter of about 50 μm, i.e., they are similar in size or slightly larger than the optically visible subgrains (15 μm–50 μm). The new grains are polygonal and optically strain-free. The recrystallized bands locally include scattered white mica and chlorite flakes, and the quartz grain boundaries are decorated with small pores (Fig. 5b).

The unrecrystallized portions of porphyroclasts contain zones of optical subgrains subparallel to adjacent recrystallized shear bands. Subgrains are also found at the tips of recrystallized zones where they terminate within the quartz porphyroclast (Fig. 5c). The unrecrystallized parts of porphyroclasts also show patchy and undulatory extinction, and deformation bands. Deformation bands are several hundreds of microns thick and are oriented at a low angle to the foliation, both in a synthetic and in an antithetic orientation relative to the sense of shear. The deformation band boundaries are irregular and strongly serrated, and are usually crosscut by arrays of recrystallized grains (Fig. 5d). Elongated porphyroclasts whose *c*-axes are subparallel to the *Y*-direction often display undulatory and patchy extinction, but a very low degree of recrystallization, the few recrystallized grains being restricted to narrow conjugate shear bands.

In samples M30G1 and M30G2 (stage 4 of deformation, 64% average grain strain), elongated monomineralic quartz domains consist of recrystallized aggregates of polygonal grains with minor unrecrystallized portions. The amount of recrystallization of each porphyroclast ranges from about 55% to 100%, with an average fraction of recrystallized grains of 85%. The average aspect ratio of the porphyroclasts is 4.6 (Fig. 3; Table 1). The unrecrystallized quartz portions show deformation lamellae, deformation bands and development of subgrains. Even at this mylonitic stage, high strain polycrystalline quartz domains are stronger than the mylonitic matrix, as shown by the common deflection of the foliation around the porphyroclasts (Fig. 5e) that locally form pinch and swell structures. Even in cases of extensive recrystallization, the arrangement of quartz grains locally still mimics the geometry of the precursory sets of conjugate shear bands, oblique to the porphyroclast elongation and to foliation (Fig. 5f). Recrystallized grains range in diameter from 10–20 μm to up to 100 μm.

4.2.2. Mylonitic quartz vein

Sample DBL2090 is a completely recrystallized sheared quartz vein transposed along the foliation of the Arolla granitoid mylonites (i.e., adjacent to samples from stage 4). The quartz grains are slightly elongated defining an oblique foliation

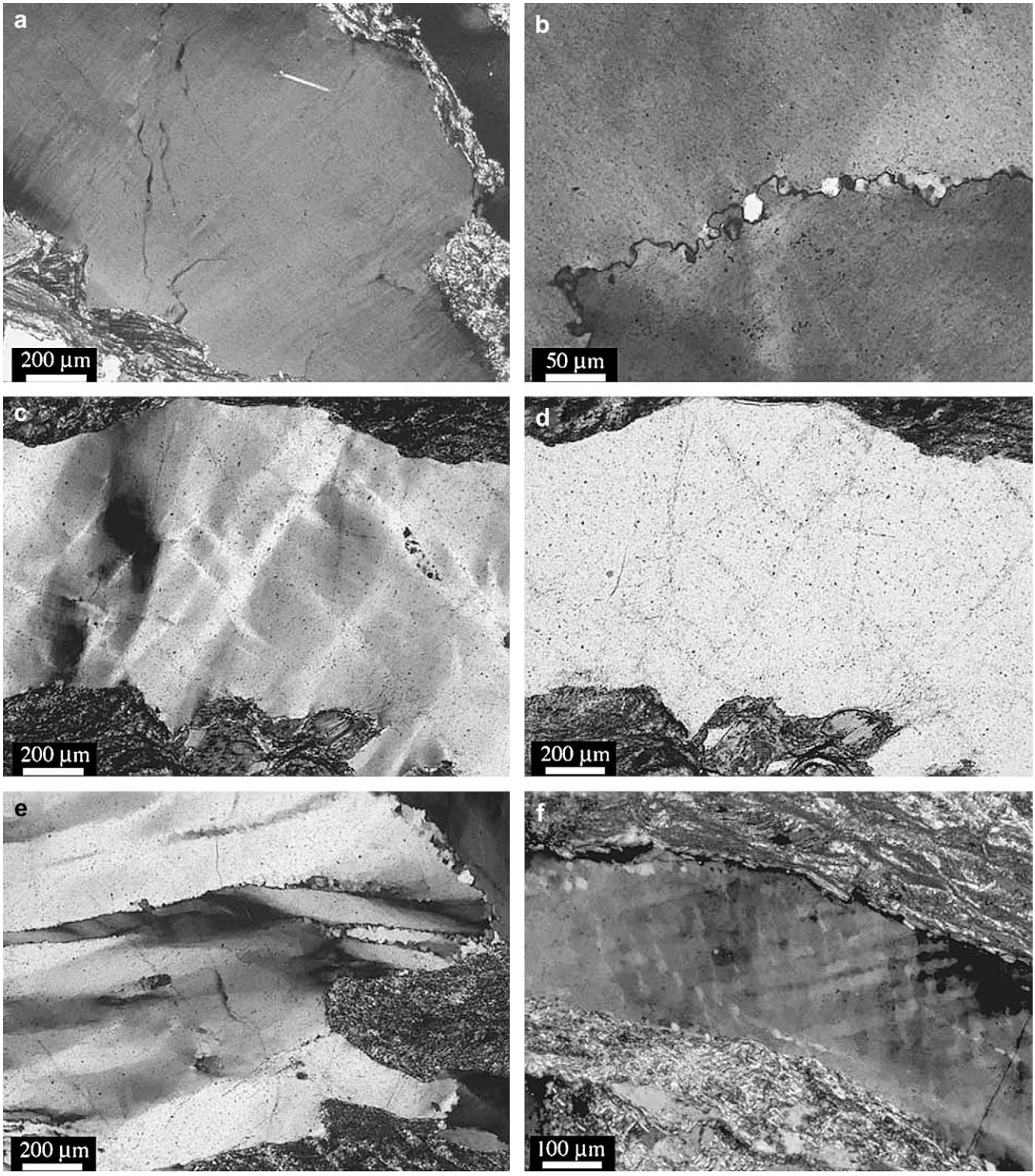

Fig. 4. Microstructures of quartz typical for stage 1 and stage 2 samples. Sense of shear is dextral, crossed polarizers. Bulk rock foliation is horizontal. (a) Stage 1: Quartz porphyroclast with deformation lamellae running ~NE–SW and undulatory extinction. (b) Stage 1: Formation of bulges at the interface between two porphyroclasts. (c) Stage 2: Conjugate shear bands intersecting at an angle of ~90° within a Z_{syn}-type quartz porphyroclast. Note the incipient recrystallization within a right-dipping shear band. The conjugate shear bands are definitely not parallel to any specific crystallographic plane. See COI and pole figure of this porphyroclast in the Supplementary material. (d) Same conjugate shear bands as in (c), but with parallel polarizers. Trails of fluid inclusions outlining the shear bands are evident. (e) Stage 2: Deformation bands at low angle to the incipient host rock foliation. Note the strongly serrated deformation band boundaries and the local incipient recrystallization. (f) Stage 2: Development of blocky subgrains within a quartz porphyroclast.

synthetically inclined at 20°–30° to the shear plane (Fig. 6). Most of the grains appear strain-free under the optical microscope and range in diameter from ~50 μm to 250 μm. Thin and discontinuous muscovite and chlorite layers are locally present along the foliation.

4.3. Quartz c-axis CPO

4.3.1. Stage 1 and stage 2 samples (U-stage data)

In weakly deformed and foliated granitoid samples (stages 1 and 2), because of the coarse grain size, several thin sections were used to

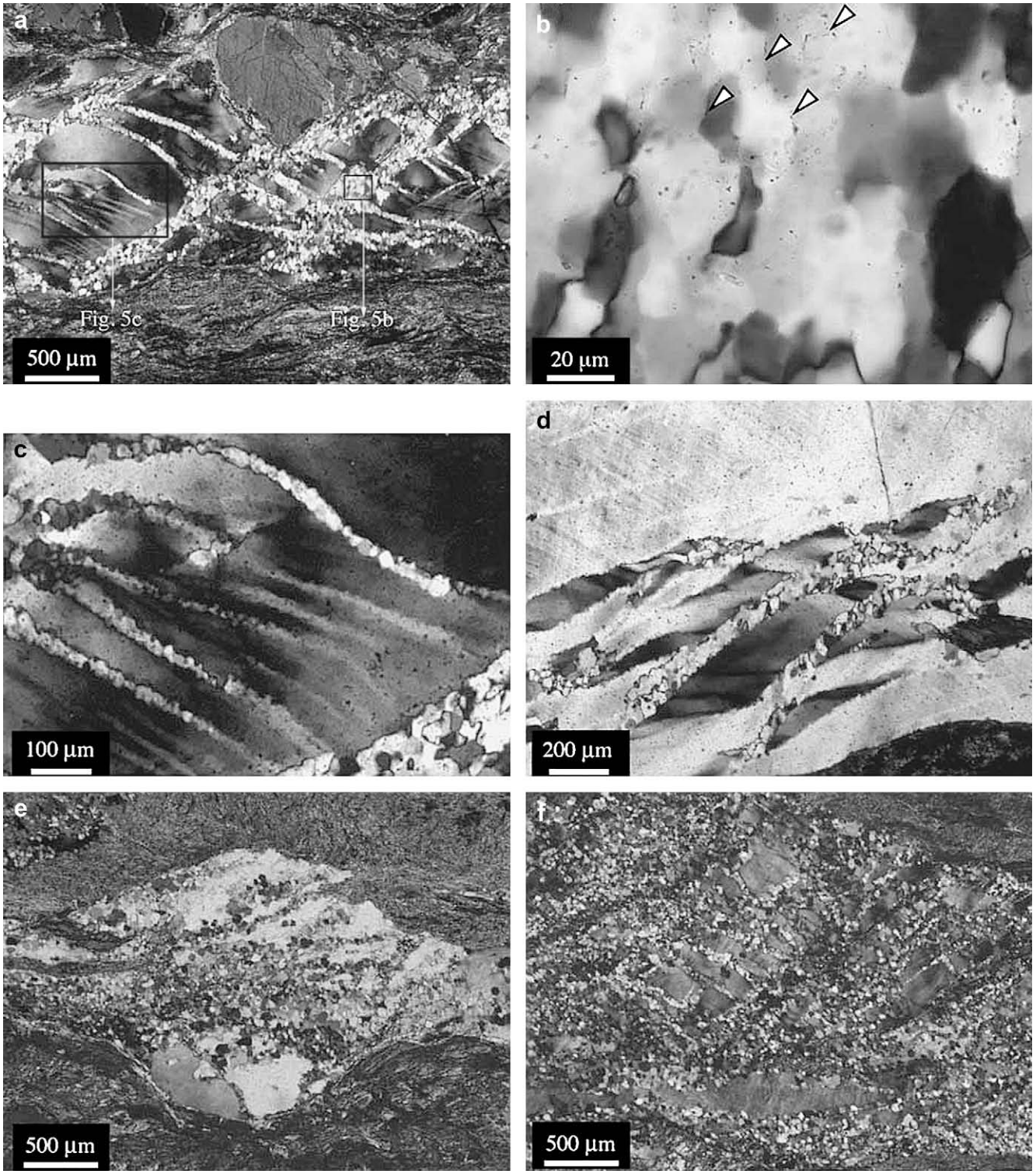

Fig. 5. Microstructures of quartz typical for stage 3 and stage 4 samples. Sense of shear is dextral, crossed polarizers, mylonitic foliation is horizontal. (a) Stage 3: Conjugate shear bands of recrystallized grains within a quartz porphyroclast with the *c*-axis subparallel to the *Z*-direction. Positions of Fig. 5b and c are shown. (b) Detail of (a): fluid inclusions, indicated by white arrowheads, decorate the boundaries of recrystallized grains within a left-dipping shear band. (c) Detail of (a): subgrains develop adjacent to the right-dipping recrystallized shear bands and at the tip of some shear bands. (d) Stage 3: Intracrystalline arrays of recrystallized grains crosscutting deformation bands at low angle to the mylonitic foliation. (e) Stage 4: Mylonitic foliation deflected around a quartz porphyroclast. (f) Stage 4: Recrystallized quartz grains developed along the precursor intracrystalline shear bands inclined to the mylonitic foliation of the granitoid.

collect a meaningful number of *c*-axis orientations of the quartz porphyroclasts. In stage 1 no CPO can be detected (Fig. 7a). In stage 2, the quartz *c*-axis CPO pattern resembles a type-I crossed girdle, but the small number of data does not allow any reliable inference about the sense of shear or the strength of the CPO (Fig. 7b).

4.3.2. Stage 3 samples (CIP data)

Because of the strong intracrystalline deformation of quartz porphyroclasts and the small size of recrystallized grains, stage 3 samples were unsuitable for U-stage measurements; instead the CIP method was used. The whole thin section and several individual

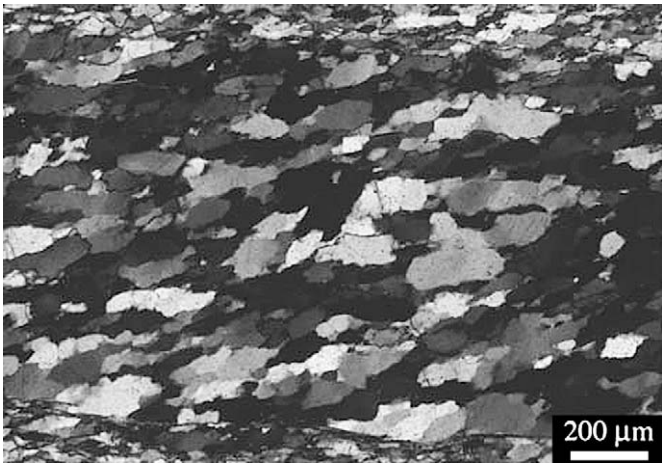

Fig. 6. Microstructure of quartz from the mylonitic quartz vein (sample DBL2090). A shape preferred orientation of the recrystallized quartz grains consistent with the dextral sense of shear is evident. Crossed polarizers.

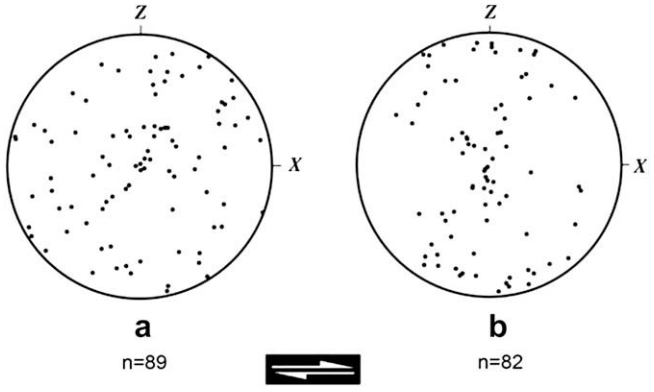

Fig. 7. U-stage measurements of the CPO of quartz porphyroclasts within stage 1 (a) and stage 2 (b) samples. Data are plotted on the upper hemisphere of the Schmidt projection.

monomineralic quartz domains were analyzed. Pole figures were obtained for the total quartz, for the recrystallized grain fraction and for the unrecrystallized portions of the porphyroclasts.

The *c*-axis orientation image (COI) and the bulk pole figure of a thin section of stage 3 are shown in Fig. 8. The pole figure is dominated by the contribution of quartz porphyroclasts, as the recrystallized grains account for only 13% of the total quartz volume. The CPO is characterized by two relatively strong maxima about the *Z*-direction, indicating intracrystalline deformation of the porphyroclasts with an alignment of the basal planes towards the foliation plane. In Fig. 8b, only a small fraction of porphyroclasts appears pink, red or yellow, indicating that most *c*-axes are at a high angle to the foliation and close to the *Z*-direction. We distinguish four "end-member" types of porphyroclasts for stage 3:

- Porphyroclasts with *c*-axes oriented orthogonal to the foliation and subparallel to the *Z*-direction, here referred to as *Z-type* porphyroclasts. They appear dominantly green and blue in Fig. 8b.
- Porphyroclasts with *c*-axes lying in the *XZ* plane and slightly inclined, antithetically and synthetically, with respect to the sense of shear (Z_{anti}*-type* and Z_{syn}*-type* porphyroclasts, respectively). These porphyroclasts have a dominant yellow and pink colour, respectively, in Fig. 8b.
- Porphyroclasts with the *c*-axes oriented off, and at a relatively high angle to, the *XZ* plane (e.g., close to *Y*), here referred to as *Y-type* porphyroclasts. They appear dominantly grey in Fig. 8b.

Examples of the four types of porphyroclasts are shown in the *c*-axis orientation images of Fig. 9. These different porphyroclast types show different degrees of recrystallization (Fig. 9), with the highest amount of recrystallized grains (43%) in the *Z-type* porphyroclast. The *Z-type* porphyroclasts show clear sets of conjugate shear bands of recrystallized grains (but one orientation dominates), symmetrically oriented with respect to the *Z*-axis, while in the other types of porphyroclasts the shear bands are generally less well-developed.

Irrespective of the *c*-axis orientation of the porphyroclast(s) depicted by the single maxima in the pole figures (Fig. 9), the CPOs of the recrystallized grains of the *Z-type*, Z_{anti}*-type* and Z_{syn}*-type* porphyroclasts are quite similar and do not seem to depend on the

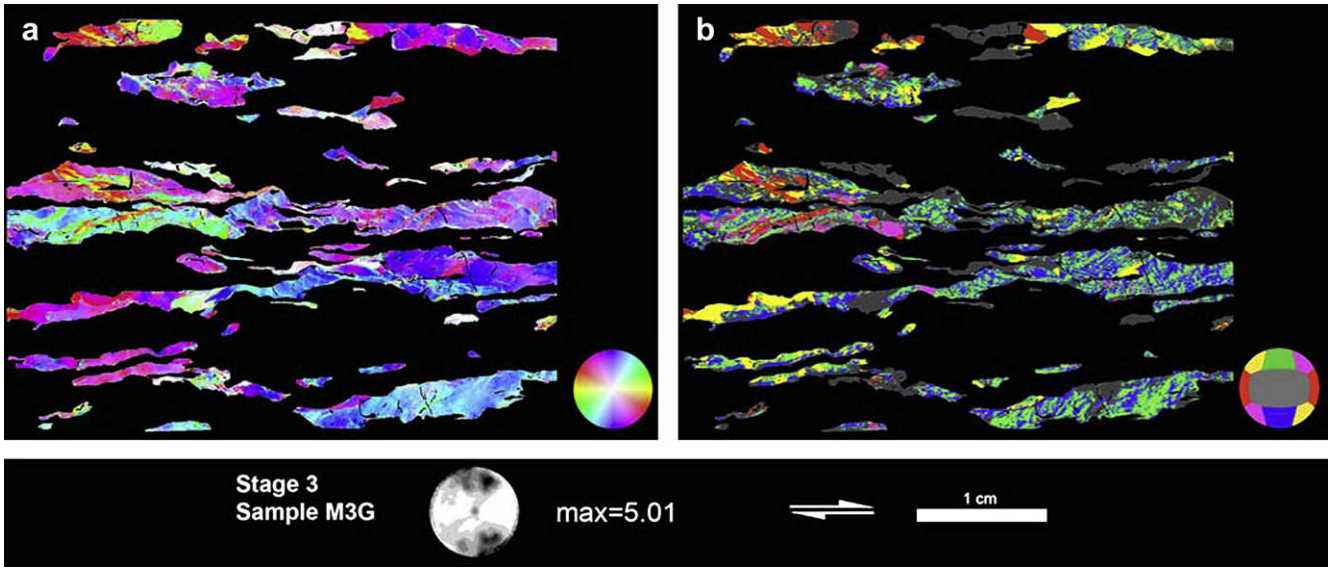

Fig. 8. CIP-derived *c*-axis orientation images (COIs) of sample M3G (stage 3 of the deformation). Colour look-up tables adopted for (a) and (b) are shown at lower right of each COI. In (b) different orientation domains are depicted by different colours (e.g., *Z*-type porphyroclasts appear green and/or blue, Z_{syn}-type appear pink, Z_{anti}-type appear yellow, *Y*-type appear grey). Total amount of recrystallization in this sample is 13%. The *c*-axis pole figure is shaded in 0.5 intervals up to four times the uniform distribution.

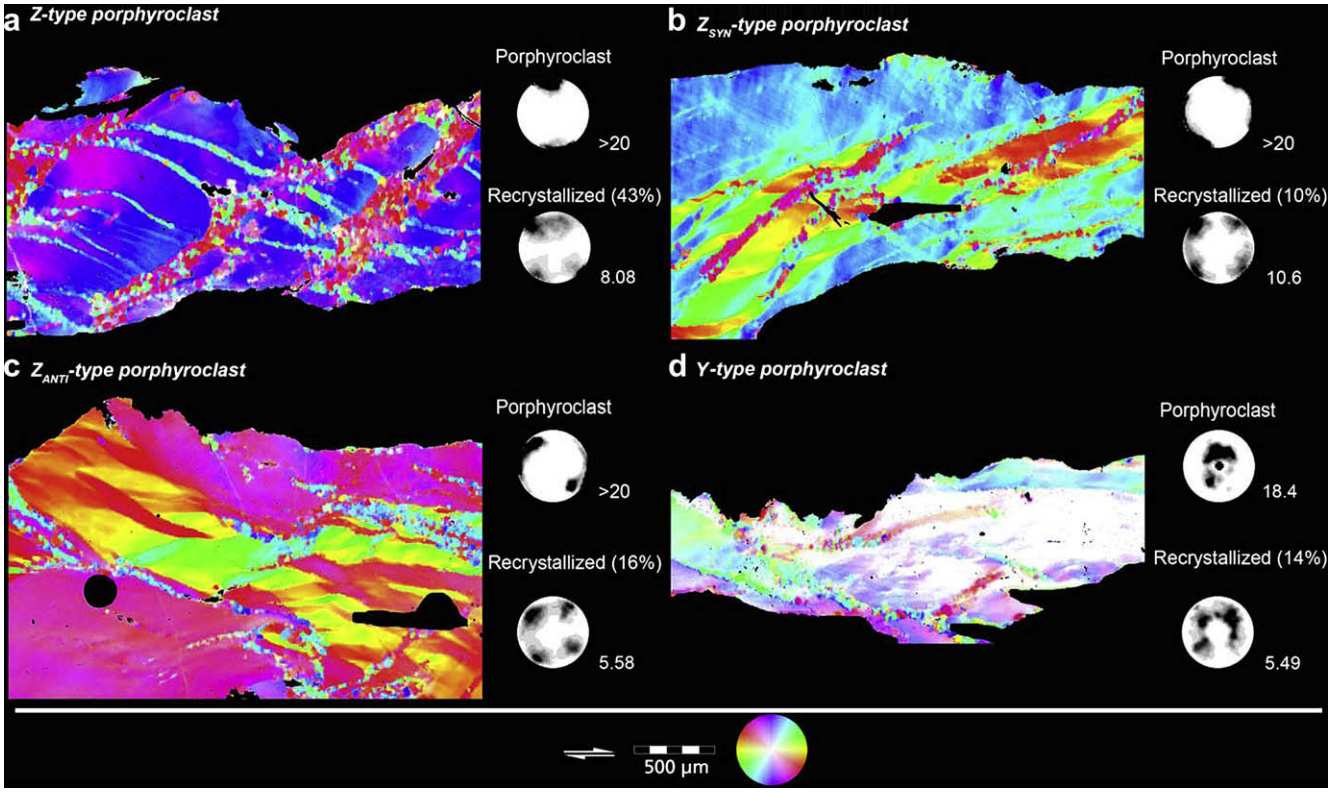

Fig. 9. CIP-derived *c*-axis orientation images of the four types of porphyroclasts in stage 3 samples. The *c*-axis pole figures of the host porphyroclasts and of the recrystallized grains are shown separately. The volume fraction of recrystallized grains within each porphyroclasts is reported inside brackets. Scale bar, sense of shear and colour look-up table apply to all samples. Contours of the pole figures are 0.5 times uniform. Maxima are indicated at lower right of pole figures.

crystallographic orientation of the host grain. Four maxima appear close to the *XZ* plane at an angle of about 45° to the *Z*-direction. In the *Y-type* porphyroclasts these maxima are spread out from the centre of the pole figure (compared to the host grain *c*-axis orientation) and symmetrically arranged with respect to the *YZ* plane, though slightly inclined to the *XZ* plane. Overall, the *c*-axis CPO patterns of the recrystallized grains suggest slip on the basal planes aligned parallel to the shear band boundaries (e.g., Vernooij et al., 2006a).

The COI for a *Z-type* porphyroclast in Fig. 9a shows that the *c*-axes of the recrystallized grains within the conjugate shear bands have an orientation suborthogonal to the shear band boundaries with a large spread of orientations, up to 60° away from the *Z*-direction, with a sharp maximum at ~45° to *Z*-direction. The same broad azimuthal range characterizes the less-developed shear bands within Z_{anti}-, Z_{syn}- and *Y-type* porphyroclasts.

Fig. 10 shows a misorientation image of a *Z-type* porphyroclast illustrating the difference between the *c*-axis orientations at each pixel with respect to the main orientation of the porphyroclast. Despite the fact that these (optical) misorientations do not represent true misorientations (Wheleer et al., 2001), a few interesting observations can be made. Along profiles that cross the recrystallized shear bands (A–A′ and B–B′ in Fig. 10b), high misorientations (up to 60°) at the shear band boundaries are visible. Comparing profiles C–C′ and D–D′ along the shear bands, it appears that the variation of orientation increases with increasing width of the shear band. It is also evident from the C–C′ and D–D′ profiles that each single new grain shows a typical high (up to 30°) misorientation with respect to the adjacent neighbour grain.

4.3.3. Stage 4 samples (CIP data)

The *c*-axis orientation image and the pole figure of a thin section of stage 4 are shown in Fig. 11. The bulk CPO shows one peripheral broad maximum rotated with the sense of shear about the positive *Z*-direction, and one maximum at about 30° to the negative *Z*-direction, antithetic with respect to the bulk sense of shear and off the periphery of the pole figure. These two stronger maxima are associated with the unrecrystallized portions of the porphyroclasts, which form about 15%–20% of the total quartz. The bulk CPO is weak and does not resemble any typical pole figures known for simple shear deformation of quartz.

In Fig. 12 the COIs of selected quartz domains are shown at higher magnifications. As the quartz is not fully recrystallized, it is still possible to recognize the four types of porphyroclasts described in stage 3 samples. The *c*-axis CPOs for the host porphyroclasts and the recrystallized grains are shown separately. In the *Z-type* porphyroclast the CPO of recrystallized grains displays a broad concentration of *c*-axes at the periphery of the pole figure, preferentially at a high angle to the *X*-direction and symmetrically distributed with respect to the *Z*-direction. In both the Z_{anti}- and Z_{syn}-*type* porphyroclasts the strongest maxima of *c*-axes of new grains tightly overlap the *c*-axis orientation of the host grain. The Z_{anti}-*type* porphyroclasts display, in addition, a weaker maximum at ~90° to the principal one thus retaining the "pseudo-orthorhombic" pattern characteristic of stage 3 samples. However, these porphyroclasts show a higher dispersion of *c*-axes of new grains compared with stage 3 samples. In *Y-type* porphyroclasts the *c*-axes of recrystallized grains form a broad single girdle, with a slight antithetic asymmetry with respect to the bulk sense of shear. The strongest maxima are inclined at ~45° to the foliation plane and have approximately the same orientation as the host grain.

Therefore, in stage 4 samples, despite the relatively high percentage of recrystallization within quartz grains and the high grain strain, the bulk CPO as well as the CPO of individual quartz domains has not acquired a clear overall asymmetry consistent with the general dextral sense of shear of the granitoid mylonite.

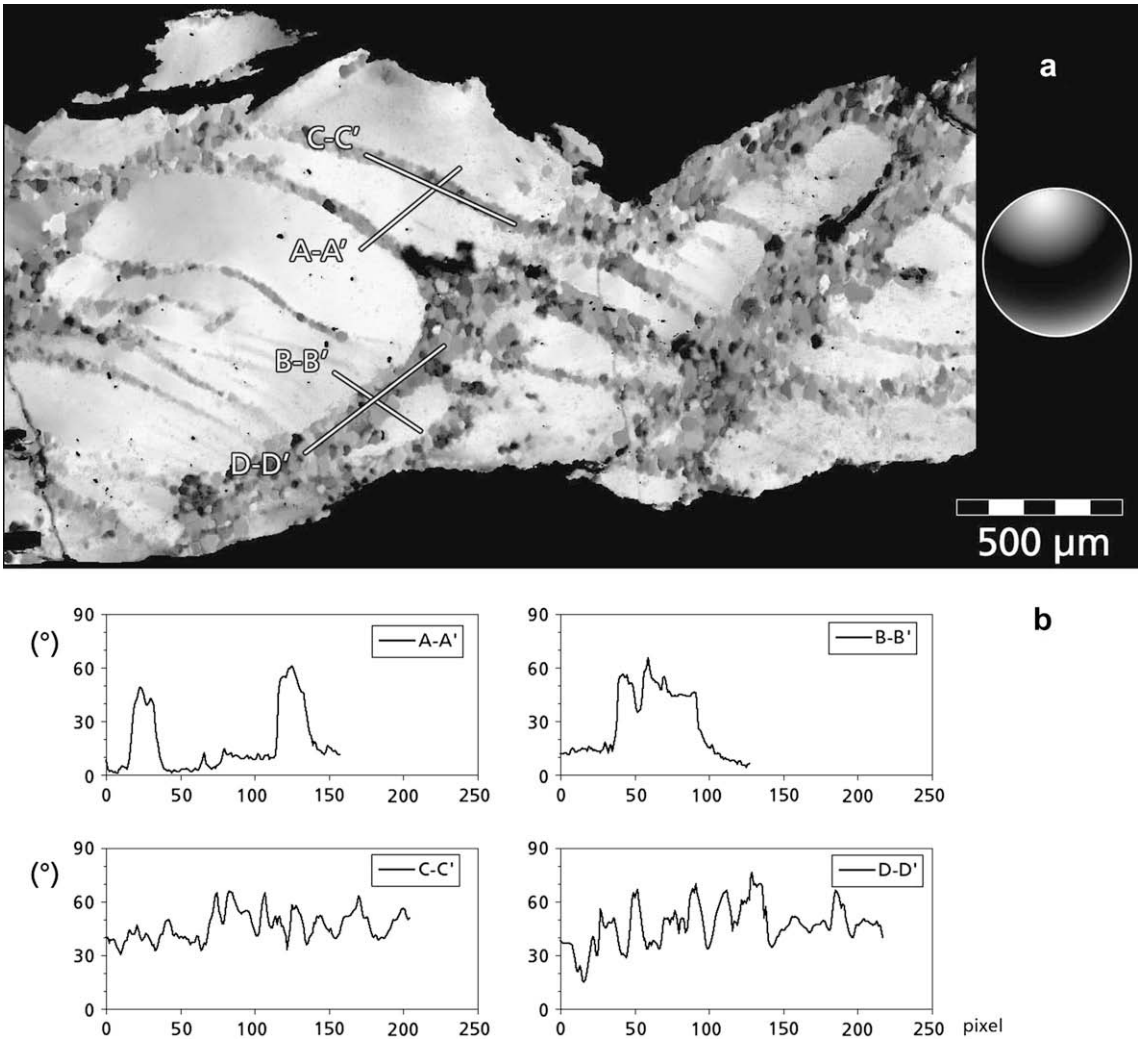

Fig. 10. CIP-derived misorientation image of the *Z*-type porphyroclast shown in Fig. 9. (a) Misorientation with respect to the average orientation (azi = 175, inc = 95, compare Fig. 9) of the porphyroclast is shown. Look-up table at right indicates white if *c*-axis is parallel to the host direction, black if *c*-axis is in plane normal to it. Locations of misorientation profiles are indicated. (b) Misorientation profiles. *X*-axis = distance in pixels (1 pixel = 2.5 microns), *Y*-axis = angular deviation from average host direction. See text for further explanation.

The *c*-axis CPOs within the individual quartz domains have not converged to any standard pattern typically found for quartz aggregates deformed under greenschist facies conditions (i.e., single or crossed girdle).

4.3.4. Mylonitic quartz vein

The *c*-axis pole figure of the mylonitic quartz vein (sample DBL2090) is shown in Fig. 13. The pattern is a single girdle synthetically inclined with respect to the sense of shear, with an incipient type-II crossed girdle and no well-defined *Y*-maximum. Such a pattern is typical for basal ⟨*a*⟩ and rhomb ⟨*a*⟩ slip, with only a minor contribution from prism ⟨*a*⟩ slip. The overall pattern is consistent with greenschist facies metamorphic conditions during deformation (Passchier and Trouw, 1996; Stipp et al., 2002).

5. Discussion

5.1. Grain-scale deformation partitioning in the Arolla granitoid and role of quartz

In the Arolla granitoids, the early breakdown of the abundant magmatic plagioclase to a fine-grained aggregate of white mica, albite and epidote produced a relatively weak matrix that became interconnected and acted as the strain-supporting framework from the very early stages of deformation. Within this matrix hornblende, K-feldspar and quartz behave as relatively 'strong' minerals and survive as more or less deformed porphyroclasts up to high bulk strain. The strong rheological contrast between the different mineral phases is likely to result in strain partitioning during bulk flow with the non-coaxial and coaxial components mainly accommodated by the weak matrix and the porphyroclasts, respectively (Bell, 1985; Passchier and Trouw, 1996; Goodwin and Tikoff, 2002; Vernon, 2004). In the Arolla deformed granitoids a dominant shear deformation of the matrix is recorded by the strong asymmetry of most fabric elements (e.g., pressure shadows and asymmetric recrystallization wings around porphyroclasts) (Pennacchioni and Guermani, 1993). Quartz behaved as a relatively hard mineral, wrapped around by the mica-rich matrix domains, and it underwent a dominant flattening strain. The coaxial deformation of quartz grains is recorded by the typical development of conjugate arrays of microfractures and shear bands symmetrically disposed with respect to the *Z*-direction. Quartz never forms highly elongated ribbons and does not evolve into an interconnected stress-supporting framework within the deforming granitoid even at relatively high longitudinal strain (64% in the mylonitic stage 4 sample).

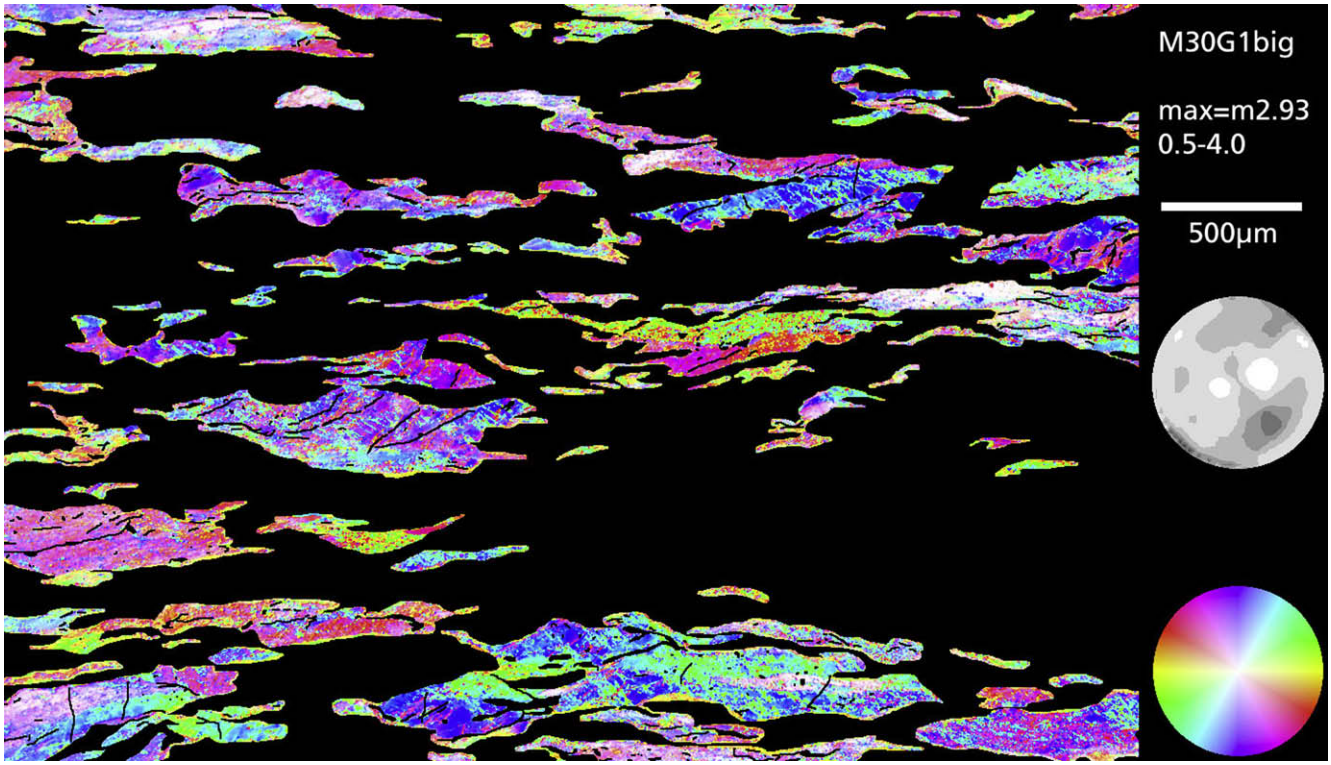

Fig. 11. CIP-derived *c*-axis orientation image (COI) of sample M30G (stage 4 of the deformation). Colour look-up table, scale and sense of shear are shown. The *c*-axis pole figure is shaded in 0.5 intervals up to four times the uniform distribution.

5.2. Brittle vs. crystal plastic deformation of quartz

Shear bands are a distinctive microstructure of quartz porphyroclasts in stage 2 to stage 4 samples. They are present in all types of quartz porphyroclasts, but they are particularly well-developed in *Z-type* ones. Recrystallized aggregates of quartz are mostly developed along these shear bands forming arrays that are one to several grains thick. The relationship between

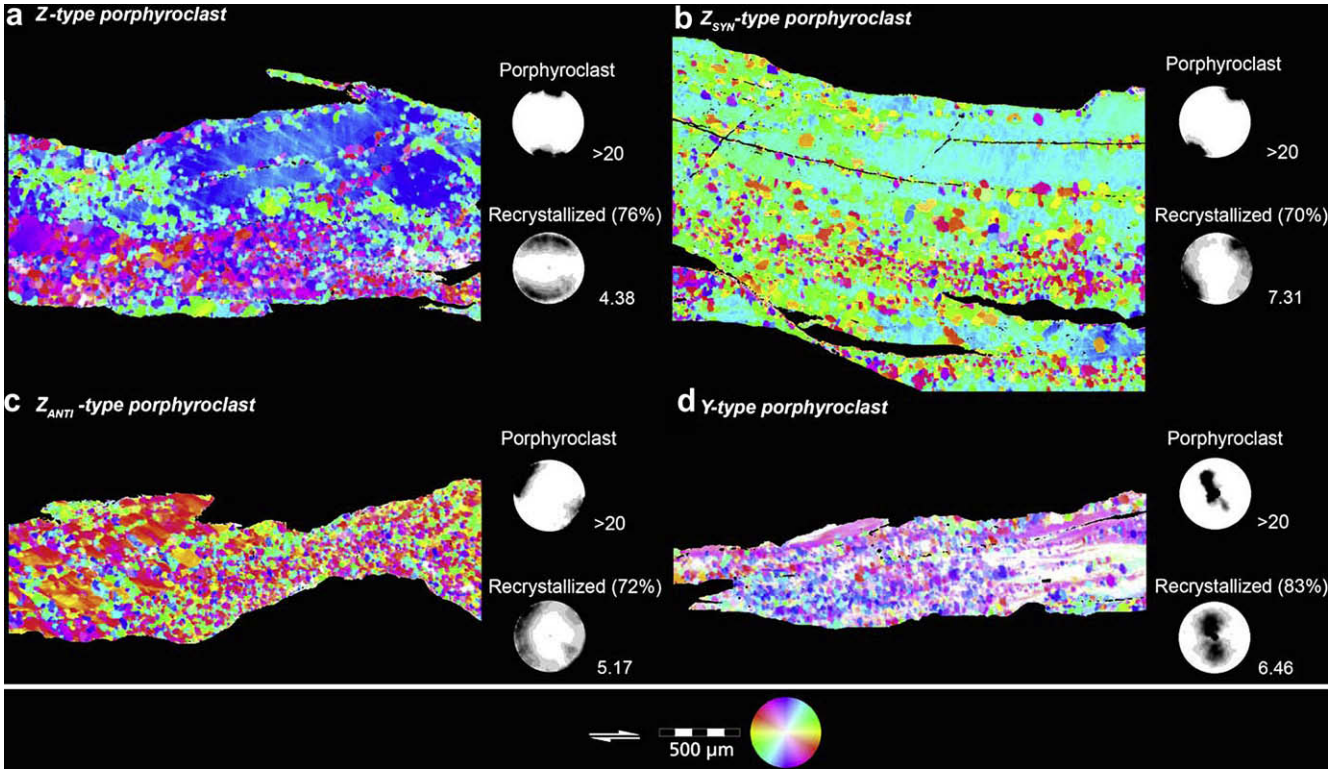

Fig. 12. CIP-derived *c*-axis orientation images of the four types of porphyroclasts in stage 4 samples. The *c*-axis pole figures of the host porphyroclasts and of the recrystallized grains are shown separately. The volume fraction of recrystallized grains within each porphyroclast is reported inside brackets. Scale bar, sense of shear and colour look-up table apply to all samples. Contours of the pole figures are 0.5 times uniform. Maxima are indicated at lower right of pole figures.

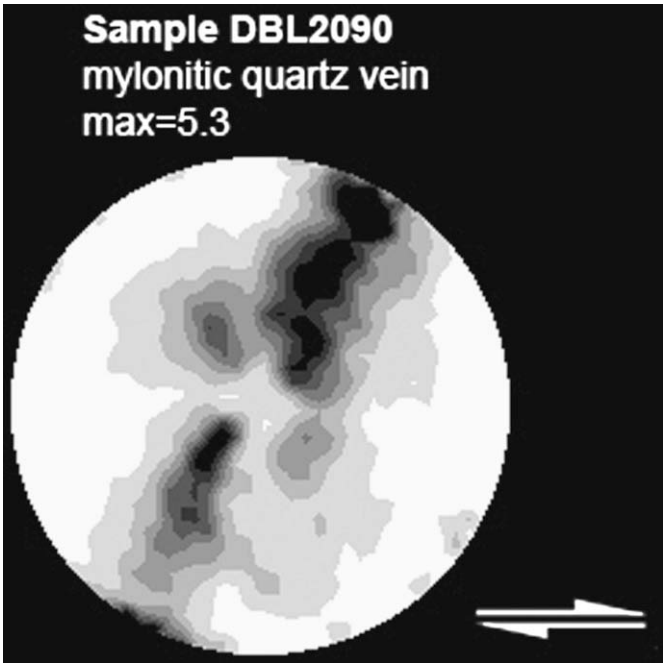

Fig. 13. *c*-axis pole figure of the mylonitic quartz vein shown in Fig. 6. Contours of the pole figure are 0.5 times the uniform distribution.

recrystallization and shear bands is still evident at high degrees of recrystallization within the mylonitic stage 4 sample (Fig. 5f). Van Daalen et al. (1999) and Vernooij et al. (2006a) observed similar recrystallized shear bands in natural quartz grains deformed under lower greenschist facies conditions and in experimentally deformed single quartz crystals, respectively. These authors relate the formation of shear bands and associated recrystallization to the initial development of shear microfractures in an orientation parallel to crystallographic rhomb planes. The development of crystallographically controlled fractures within quartz has also been observed at higher metamorphic temperatures by Vollbrecht et al. (1999).

A prominent role of microfracturing in the initiation of shear bands within the quartz porphyroclasts of the Arolla granitoid mylonites is suggested by the presence of fluid inclusion trails (healed microcracks) subparallel to the shear bands or directly marking the midline of the shear bands in stage 2 and 3 samples (Fig. 4c and d). The well-developed sets of conjugate microfractures in *Z-type* porphyroclasts, symmetrically arranged with respect to the *Z*-direction, can be explained by fracturing of the host grain along rhomb planes. The symmetric arrangement of microfractures also reflects the dominantly coaxial component of deformation within the quartz porphyroclasts. However, similar conjugate sets of shear bands symmetrically arranged to the *Z*-direction also occur in porphyroclasts different from *Z-type*, indicating that they are not always associated with fracturing along rhomb planes (Fig. 4c and Supplementary material). This observation is in contrast to the experimental results of Vernooij et al. (2006a) where conjugate intracrystalline shear zones developed only in single quartz crystals that were uniaxially compressed parallel to ⟨*c*⟩, that is, only in samples comparable with the *Z-type* porphyroclasts of the Arolla deformed granitoids.

The development of microcracks within quartz porphyroclasts may be due to strain hardening during the initial stages of plastic deformation as indicated by the widespread undulatory and patchy extinction within the porphyroclasts (Fig. 8b). In stage 2 of deformation, formation of subgrains and recrystallized grains is only at a local scale, perhaps indicating that recovery is not efficient enough to avoid build-up of dislocations and consequent hardening and fracturing. Fracturing enhances penetration into grains of fluids, whose catalytic effect in promoting recrystallization and crystal plastic deformation is well known from experimentally (e.g., Blacic and Christie, 1984) and naturally (e.g., Kronenberg et al., 1990; Mancktelow and Pennacchioni, 2004) deformed rocks. Indeed, a relationship between fracturing, fluid infiltration and the formation of intracrystalline arrays of recrystallized grains is well documented in a number of studies, both on naturally (Hippertt and Egydio-Silva, 1996; Van Daalen et al., 1999) and experimentally deformed quartz (Den Brok, 1992; Vernooij et al., 2006a,b). Recrystallization along precursor microcracks in the Arolla samples is also suggested by the occurrence of layers of new grains cross-cutting deformation bands. After initial dislocation glide (producing deformation bands), porphyroclasts were strain-hardened and underwent brittle cracking that localized fluid-assisted recrystallization.

Microfracturing is probably not the only efficient mechanism of fluid penetration. Crystal plastic processes, and subgrain rotation recrystallization in particular, may act in parallel with microcracking to produce fluid redistribution within the quartz porphyroclasts (Fitz Gerald et al., 2006). Whatever the dominant mechanism of fluid infiltration into porphyroclasts, it seems that recrystallization along shear bands occurred in the presence of a free fluid phase. Evidence includes the presence of scattered muscovite and chlorite grains along the recrystallized shear bands and pervasive fluid inclusions decorating the boundaries of the recrystallized grains within the shear bands (Fig. 5b). Once formed, the recrystallized aggregates would provide an enhanced pathway for fluid infiltration along shear bands, due to the high grain boundary permeability of fine-grained aggregates (Farver and Yund, 1991; Mancktelow and Pennacchioni, 2004).

5.3. *Progressive development of quartz* c*-axis CPO in the deformed granitoids*

This study shows a complex evolution of transient microstructures and CPOs of quartz as a function of the crystallographic orientation and accumulated strain of the porphyroclasts. In the most intensely deformed granitoids (stage 4), where the bulk strain can be reasonably assumed to be high, quartz has not yet completely recrystallized and has not developed a mature crystallographic fabric. Even where the recrystallization of quartz is total there is still a strong control of the CPO by the original grain orientation, and the CPO patterns do not reflect the bulk kinematic framework.

In the early stages (stage 2; 50% longitudinal strain), the deformation of quartz is accomplished by crystal plastic processes associated with minor microfracturing and without any significant recrystallization. Most of the bulk deformation is partitioned into the soft plagioclase-derived matrix that completely embeds the quartz grains. The microstructures (undulose and patchy extinction, microfracturing) suggest strain hardening during these initial stages of deformation. Only locally are optical subgrains developed, associated with microfractures, indicating minor and local recovery. This association was also observed by Den Brok (1992), in experimental deformation axial compression of quartz aggregates, and by Trepmann et al. (2007) in quartz deformed both naturally and experimentally at high stress. Our study, only based on light microscopy, cannot provide a definite explanation for the mechanism of subgrain formation, but the common arrangement of blocky subgrains along conjugate strips suggests that we cannot rule out that microcracking enhanced fluid access and played an important role in subgrain development in quartz from the Arolla granitoids.

During the stage 2 of deformation, the quartz grains developed a weak crossed girdle pattern of *c*-axes (Fig. 7b) from the initial random orientation (Fig. 7a). In the experiments of Dell'Angelo and Tullis (1986) quartz within deformed aplite developed a clear *c*-axis CPO already for grain strain of about 24%, i.e., at a much lower grain strain than that in stage 1 and 2 samples of the Arolla granitoids. In stage 1 Arolla samples, at a grain strain of 40%, the quartz porphyroclasts are dispersed in the plagioclase-derived matrix and no discernible *c*-axis CPO develops. In the absence of syndeformational metamorphic reaction of plagioclase, quartz becomes increasingly interconnected at about 40% grain strain in experimentally deformed aplite and has a clear CPO (Dell'Angelo and Tullis, 1986). We, therefore, infer that the 'delayed' development of *c*-axis CPO in the Arolla granitoids is due to the early decomposition of plagioclase that imposes a strong grain-scale strain partitioning, hence leaving quartz grains as relatively less deformed objects within the flowing weak matrix. This interpretation is in agreement with the results of axial compression experiments of Tullis and Wenk (1994) on synthetic aggregates of quartz and muscovite, where quartz was deformed in regime 1 and regime 2 of dislocation creep (Hirth and Tullis, 1992). The experiments demonstrate that (1) quartz grain strain, (2) percentage of recrystallization and (3) strength of quartz CPO are all significantly reduced with increasing muscovite amount due to strain partitioning.

The bulk pole figure of stage 3 sample is still dominated by the contribution of porphyroclasts (Fig. 8), and shows a maximum of *c*-axes at a high angle to the foliation, consistent with basal ⟨*a*⟩ slip as expected for greenschist facies mylonites (Passchier and Trouw, 1996; Stipp et al., 2002). The *c*-axis CPO of the recrystallized grains in *Z-type*, Z_{anti}*-type* and Z_{syn}*-type* porphyroclasts has a strong maximum approximately orthogonal to the shear band boundaries (Fig. 9), irrespective of the orientation of the host grains. Because of the common occurrence of conjugate sets of shear bands, the resulting cumulative pole figure is characterized by peripheral maxima symmetrically arranged in the *XZ* plane at an angle of ~45° to the *Z*-direction. The symmetry of the CPO depends only on the orientation of the shear bands. The microstructure and CPO of these recrystallized shear bands are very similar to those observed in quartz grains deformed under subgreenschist facies conditions (Van Daalen et al., 1999) and to those developed during experimental deformation of quartz single crystals (Vernooij et al., 2006a,b). In these studies it was inferred that the CPO of the recrystallized aggregates reflects basal slip of originally randomly oriented new fragments parallel to the shear band boundary. In the *Y-type* porphyroclasts the recrystallized grains have a slightly different CPO, but still show an "orthorhombic" symmetry. If the CPOs of the individual shear bands are rotated into a horizontal orientation (having a consistent sense of shear), the patterns show high densities in orientations suitable for basal and rhomb slip.

The recrystallization mechanism along the shear bands is difficult to assess. The misorientation profiles across the recrystallized shear bands in a *Z-type* porphyroclast are characterized by large angles (Fig. 10) at the shear band boundaries (up to 60°). A similar observation was also made by Van Daalen et al. (1999), Vernooij et al. (2006a) and Trepmann et al. (2007), who inferred that the recrystallization mechanism along the shear bands was different from progressive subgrain rotation. The Arolla granitoids are similar in that the regions adjacent to recrystallized shear bands do not show subgrain polygonization, or if they do, the subgrain misorientation is not progressive towards the shear band. Van Daalen et al. (1999) and Vernooij et al. (2006a,b) suggested that misorientation discontinuities are due to the rotation of fractured fragments and subsequent recrystallization (Van Daalen et al., 1999), or the preferred growth of new quartz grains from aqueous solution along microcracks (Vernooij et al., 2006a,b). Submicron sized and randomly oriented quartz particles within the 0.5 μm wide damage zone of some shear fractures within experimentally deformed quartz polycrystals have been observed with the TEM by Trepmann et al. (2007). Such particles might have provided nuclei for subsequent dynamic recrystallization. Trepmann et al. (2007) proposed that not only shear fractures but also deformation bands (with a high dislocation density) formed at an early stage of the deformation were potential nucleation sites for subsequent recrystallization of new grains suitably oriented for basal slip. Although also in the Arolla granitoids a precursor stage of microcracking most likely provided the preferred sites for successive recrystallization along shear bands, some observations suggest that subgrain rotation played some role during recrystallization: (i) the recrystallized grain size within shear bands is uniform and the same or larger than the subgrain size; (ii) layers of optical subgrains (with a thickness of a single subgrain) can be found within the unrecrystallized portion of porphyroclasts subparallel to adjacent recrystallized shear bands (Fig. 5c) or at the tip of the recrystallized bands.

Most likely, fluids played a prominent role during shear band recrystallization. New high angle grain boundaries developed by progressive subgrain rotation promote fluid infiltration into the core of quartz porphyroclasts: TEM observations in quartz mylonites indicate that the transition from subgrain to new high angle grain boundaries is marked by the appearance of grain boundary fluid inclusions that are conspicuously absent along subgrains (Fitz Gerald et al., 2006). The presence of grain boundary fluids along recrystallized shear bands is well documented in our samples by the localized fluid inclusion trails.

During stage 4, there is pervasive recrystallization of the porphyroclasts and the volume of new grains is up to 85% of the total volume of quartz. At this stage, corresponding to a maximum extension of 110% and a longitudinal strain of 64%, the pole figures of the recrystallized grains show a clear host-control with broad *c*-axis maxima overlapping the *c*-axis orientation of the host grain (Fig. 12). In porphyroclasts not fully recrystallized, some recrystallized aggregates locally still show a geometric relationship with the conjugate sets of shear bands (Fig. 5f), but the bulk CPO of the recrystallized grains is not related to the kinematics of slip along the shear bands as in the case of stage 3. Instead, host-control and dispersion of CPO maxima are typical of subgrain rotation recrystallization. Continued recrystallization of shear bands promotes the partitioning of shear strain along the fine-grained "hydrated" aggregates of recrystallized quartz. Strain accumulation along the network of internal recrystallized microshear zones implies a strong distortion on the porphyroclast fragments between the shear bands, as conjugate shear bands tend to rotate with increasing deformation (Mancktelow, 2002). The rotation of conjugate shear bands leads to a spread of deformation throughout the whole porphyroclasts at higher strain (stage 4), which is manifested in the diffuse subgrain polygonization and subgrain rotation recrystallization. Both are promoted by fluid influx into the porphyroclasts. We infer that the switch from a 'shear band-controlled' to a 'host-controlled' *c*-axis CPO of recrystallized grains at around 64% grain strain reflects the onset of pervasive subgrain rotation recrystallization within the porphyroclasts. This switch seems to occur for an amount of recrystallization between 40% (when the *c*-axis CPO is still 'shear band-controlled', although the paired maxima are progressively converging into a single broad maximum coincident with the host orientation, Fig. 9a) and 70% (when a clear host-control is observed, Fig. 12).

The host-control on the CPO of recrystallized grains at stage 4 implies that the asymmetry of CPO of recrystallized quartz aggregates cannot be used at this mylonitic stage to infer the kinematics of the bulk deformation. The bulk pole figure for the whole thin section of the mylonitic stage 4 sample (Fig. 11) is not similar to any standard *c*-axis pattern for high strain simple shear characteristic of greenschist facies, and does not show any asymmetry indicative of the bulk

sense of shear. All that can be inferred from the absence of a clear *c*-axis pattern is the notion that in Arolla granitoids the establishment of a steady state deformation microstructure and CPO of quartz is hindered by the strain partitioning between quartz and mica-rich matrix, which lowers the quartz phase strain by decreasing quartz–quartz grain contacts (e.g., Tullis and Wenk, 1994).

5.4. Comparison with a pure quartz mylonite

The studied quartz mylonite (sample DBL2090, Fig. 6) is a very thin recrystallized vein that lies parallel to the main mylonitic foliation of the granitoids. It has a CPO with an asymmetric single girdle distribution synthetically inclined with respect to the bulk shear sense (Fig. 13). Individual maxima of the CPO suggest basal and rhomb slip, with minor activity of the prism ⟨*a*⟩ slip system. Such a *c*-axis CPO pattern is common in quartz mylonites deformed under greenschist facies conditions (Schmid and Casey, 1986; Passchier and Trouw, 1996; Stipp et al., 2002).

In the absence of a quantitative estimate of the strain of the quartz mylonite relative to the quartz grains within the granitoid mylonites we can only speculate about the reasons for this difference between the quartz CPO within the monomineralic (quartz vein) and that of polymineralic (granitoid) rock. One interpretation of this difference is that the CPO in the quartz vein just represents a higher strain, "steady state" type compared to the one observed in the mylonitic granitoids. Because of its tabular (i.e., high aspect ratio) geometry, quartz veins lying parallel to the mylonitic foliation are less prone to strain partitioning and may undergo non-coaxial deformation from the initial stages, just as the surrounding granitoid mylonites. The mature *c*-axis pattern observed in the quartz mylonite might reflect strain localization within the veins hosted in granitoids, as described at temperatures >400 °C–450 °C in the Adamello pluton and in the Tauern Window of the Eastern Italian Alps (Pennacchioni, 2005; Pennacchioni and Mancktelow, 2007). However, this localization commonly occurs under conditions where plagioclase is stable and quartz behaves as a weak phase. The Arolla granitoids, where plagioclase is unstable and reacts to a soft matrix, are clearly different. Therefore, in the Arolla the strain accumulated within the quartz vein is likely of the same order of magnitude, or even less, that that in the granitoid mylonites. Hence, the difference in quartz *c*-axis CPO more likely reflects a difference in strain path experienced by quartz grains in the granitoids (i.e., dispersed porphyroclasts undergoing dominantly coaxial strain) and in the quartz mylonites (monomineralic aggregate undergoing dominantly non-coaxial strain).

6. Conclusions

The microstructural and quartz *c*-axis CPO analyses on a sample suite representative of four stages of increasing ductile shear deformation of granitoids from the Arolla unit of the Western Italian Alps lead to the following conclusions:

1. The early decomposition of plagioclase into a weak matrix of albite, white mica and epidote resulted in a strong grain-scale strain partitioning that left quartz as a relatively 'hard' phase, which underwent dominantly coaxial strain throughout the whole deformation history.
2. The deformation partitioning had a major effect on the evolution of quartz microstructures and *c*-axis CPOs, because the quartz grains remained dispersed and less strained. As a consequence, the development of a quartz *c*-axis CPO is strongly delayed with respect to the quartz aplite experimentally deformed at high temperature by Dell'Angelo and Tullis (1986) (characterized by similar amounts of quartz and feldspars as in the Arolla granitoid), where quartz behaved as the weak phase. Much more grain strain (up to 50% compared to 22% in the aplite) is required in the Arolla granitoids in order for quartz porphyroclasts to develop a clear *c*-axis CPO.
3. The *c*-axis CPO of recrystallized quartz is characterized by transient stages, related to the amount of recrystallization and to the orientation of the original porphyroclast. No host-control on the *c*-axis orientation of recrystallized grains occurred at relatively low amounts of recrystallization (<50%) and up to 60% of grain strain. Independent of the orientation of the porphyroclast, recrystallized grains localize along intracrystalline shear bands and have a *c*-axis CPO with a pseudo-orthorhombic symmetry related only to the orientation of the shear band itself. Most likely, shear bands developed from shear microcracks that do not appear to nucleate selectively along the rhomb plane. A mature *c*-axis CPO of recrystallized quartz grains is not attained even at large amounts of recrystallization (up to 85%) and grain strain (64%). The clear host-control on the *c*-axis CPO of recrystallized grains in stage 4 samples indicates that progressive subgrain rotation was the dominant recrystallization mechanism. The switch between 'shear band-controlled' to 'host-controlled' *c*-axis CPO occurred between 40% and 70% of recrystallization.
4. The absence of a clear and mature *c*-axis CPO implies that the asymmetry of CPO patterns of recrystallized quartz aggregates cannot be used within the Arolla mylonitic granitoid to infer the kinematics of the bulk deformation. Therefore, within a polymineralic rock where most of the deformation is partitioned to other sites, quartz microstructures and CPOs may not be representative of the bulk kinematics even at high grain strain values.
5. The quartz *c*-axis CPO within a fully recrystallized quartz vein transposed along the mylonitic foliation of the granitoids shows a single girdle pattern, consistent with greenschist facies deformation conditions. This pattern indicates that the CPO evolution of quartz may significantly differ in cases of polymineralic vs. monomineralic rocks under the same deformation conditions, if most of the deformation of the polyphase rock is partitioned in other mineral phases.

Acknowledgements

The research was funded by the University of Padova: Ricerca Scientifica fondi quota ex 60% (60A05-3129/05 and 60A05-3770/06). For the digital image analysis the free software ImageSXM (http://www.liv.ac.uk/~sdb/ImageSXM/) was used. We wish to thank Holger Stünitz for insightful discussions and Richard Spiess for his comments on an earlier version of the manuscript. Jan Tullis is warmly acknowledged for her very constructive and thorough review. LM is grateful for financial support by an A. Gini Foundation research grant during his stay at Basel University. This paper is dedicated to our friend James MacKenzie, whom we will never forget.

Appendix. Supplementary material

Supplementary material for this article may be found, in the online version, at doi: 10.1016/j.jsg.2008.07.007.

References

Bell, T.H., 1985. Deformation partitioning and porphyroblast rotation in metamorphic rocks: a radical reinterpretation. Journal of Metamorphic Geology 3, 109–118.

Blacic, J.D., Christie, J.M., 1984. Plasticity and hydrolytic weakening of quartz single crystals. Journal of Geophysical Research 89, 4223–4239.

Cladouhos, T.T., 1999. Shape preferred orientations of survivor grains in fault gouge. Journal of Structural Geology 21, 419–436.
Dal Piaz, G.V., Hunziker, J.C., Martinotti, G., 1972. La Zona Sesia-Lanzo e l'evoluzione tettonico-metamorfica delle Alpi nordoccidentali interne. Memorie della Società Geologica Italiana 11, 433–466.
Dell'Angelo, L.N., Tullis, J., 1986. A comparison of quartz *c*-axis preferred orientations in experimentally deformed aplites and quartzites. Journal of Structural Geology 8, 683–692.
Dell'Angelo, L.N., Tullis, J., 1996. Textural and mechanical evolution with progressive strain in experimentally deformed aplite. Tectonophysics 256, 57–82.
Den Brok, B., 1992. An experimental investigation into the effect of water on the flow of quartzite. Geologica Ultraiectina 95, 1–178.
Dunlap, W.J., Hirth, G., Teyssier, C., 1997. Termomechanical evolution of a ductile duplex. Tectonics 16, 983–1000.
Farver, J.R., Yund, R.A., 1991. Measurement of oxygen grain boundary diffusion in natural, fine-grained, quartz aggregates. Geochimica et Cosmochimica Acta 55, 1597–1607.
Fitz Gerald, J.D., Stünitz, H., 1993. Deformation of granitoids at low metamorphic grade I: reactions and grain size reduction. Tectonophysics 221, 269–297.
Fitz Gerald, J.D., Mancktelow, N.S., Pennacchioni, G., Kunze, K., 2006. Ultra-fine grained quartz mylonites from high-grade shear zones: evidence for strong dry mid-to-lower crust. Geology 34, 369–372.
Gapais, D., 1989. Shear structures within deformed granites: mechanical and thermal indicators. Geology 17, 1144–1147.
Gleason, G.C., Tullis, J., Heidelbach, F., 1993. The role of dynamic recrystallization in the development of lattice preferred orientations in experimentally deformed quartz aggregates. Journal of Structural Geology 15, 1145–1168.
Goodwin, L.B., Tikoff, B., 2002. Competency contrast, kinematics, and the development of foliations and lineations in the crust. Journal of Structural Geology 24, 1065–1085.
Gueydan, F., Leroy, Y.M., Jolivet, L., Agard, P., 2003. Analysis of continental mid-crustal strain localization induced by microfracturing and reaction-softening. Journal of Geophysical Research 108 (B2), 2064, doi:10.1029/2001JB000611.
Handy, M.R., 1990. The solid-state flow of polymineralic rocks. Journal of Geophysical Research 95 (B), 8647–8661.
Heilbronner, R., 2000. Optical orientation imaging. In: Jessel, M.W., Urai, J.L. (Eds.), Stress, Strain and Structure, a Volume in Honouxr of W.D. Means. Journal of the Virtual Explorer, 2. <http://virtualexplorer.com.au/VEjournal/Volume 2/>.
Heilbronner, R., Tullis, J., 2002. The effect of static annealing on microstructure and crystallographic preferred orientation of quartzites experimentally deformed in axial compression and shear. In: de Meer, S., Drury, M.R., de Bresser, J.H.P., Pennock, G.M. (Eds.), Deformation Mechanisms, Rheology and Tectonics: Current Status and Future Perspectives. Geological Society of London, Special Publication, vol. 200, pp. 191–218.
Heilbronner, R., Tullis, J., 2006. Evolution of c axis pole figures and grain size during dynamic recrystallization: results from experimentally sheared quartzite. Journal of Geophysical Research 111, B10202, doi:10.1029/2005JB004194.
Hippertt, J.F., 1998. Breakdown of feldspar, volume gain and lateral mass transfer during mylonitization of granitoid in a low metamorphic grade shear zone. Journal of Structural Geology 20, 175–193.
Hippertt, J.F., Egydio-Silva, M., 1996. New polygonal grains formed by dissolution–redeposition in quartz mylonite. Journal of Structural Geology 18, 1345–1352.
Hirth, G., Tullis, J., 1992. Dislocation creep regimes in quartz aggregates. Journal of Structural Geology 14, 145–159.
Holyoke, C.W., Tullis, J., 2006. Mechanisms of weak phase interconnection and the effects of phase strength contrast on fabric development. Journal of Structural Geology 28, 621–640.
Kronenberg, A.K., Segall, P., Wolf, G.H., 1990. Hydrolytic weakening and penetrative deformation within a natural shear zone. In: Duba, A.G., Durham, W.B., Handin, J.W., Wang, H.F. (Eds.), The Brittle–Ductile Transition in Rocks: the Heard Volume. American Geophysical Union, Geophysical Monograph, vol. 56, pp. 21–36.
Law, R.D., 1990. Crystallographic fabrics: a selective review of their applications to research in structural geology. In: Knipe, R.J., Rutter, E.H. (Eds.), Deformation Mechanisms, Rheology and Tectonics. Geological Society of London, Special Publication, vol. 54, pp. 819–834.
Lister, G.S., Hobbs, B.E., 1980. The simulation of fabric development during plastic deformation and its application to quartzite: the influence of deformation history. Journal of Structural Geology 2, 355–370.
Lister, G.S., Williams, P.F., 1983. The partitioning of deformation in flowing rock masses. Tectonophysics 92, 1–33.
Mancktelow, N.S., 1987. Atypical textures in quartz veins from the Simplon Fault Zone. Journal of Structural Geology 9, 995–1005.
Mancktelow, N.S., 2002. Finite-element modelling of shear zone development in viscoelastic materials and its implications for localisation of partial melting. Journal of Structural Geology 24, 1045–1053.
Mancktelow, N.S., Pennacchioni, G., 2004. The influence of grain boundary fluids on the microstructure of quartz–feldspar mylonites. Journal of Structural Geology 26, 47–69.
Panozzo Heilbronner, R., Pauli, C., 1993. Integrated spatial and orientation analysis of quartz *c*-axes by computer-aided microscopy. Journal of Structural Geology 15, 369–382.
Park, Y., Yoo, S.-H., Ree, J.-H., 2006. Weakening of deforming granitic rocks with layer development at middle crust. Journal of Structural Geology 28, 919–928.
Passchier, C.W., Trouw, R.A.J., 1996. Microtectonics. Springer-Verlag, Heidelberg.
Pauli, C., Schmid, S.M., Panozzo Heilbronner, R., 1996. Fabric domains in quartz mylonites: localized three dimensional analysis of microstructure and texture. Journal of Structural Geology 18, 1183–1203.
Pennacchioni, G., 2005. Control of the geometry of precursor brittle structures on the type of ductile shear zone in the Adamello tonalites, Southern Alps (Italy). Journal of Structural Geology 27, 627–644.
Pennacchioni, G., Guermani, A., 1993. The mylonites of the Austroalpine Dent Blanche nappe along the northwestern side of the Valpelline Valley (Italian Western Alps). Memorie di Scienze Geologiche 45, 37–55.
Pennacchioni, G., Mancktelow, N.S., 2007. Nucleation and initial growth of a shear zone network within compositionally and structurally heterogeneous granitoids under amphibolite facies conditions. Journal of Structural Geology 29, 1757–1780.
Sander, B., 1950. Einführung in die Gefügekunde der geologischen Körper, zweiter Teil: Die Korngefüge. Springer, Wien.
Schmid, S.M., Casey, M., 1986. Complete fabric analysis of some commonly observed quartz [c]-axis patterns. In: Hobbs, B.E., Heard, H.C. (Eds.), Mineral and Rock Deformation: Laboratory Studies. American Geophysical Union, Geophysical Monograph, vol. 36, pp. 263–286.
Shea, W.T., Kronenberg, A.K., 1993. Strength and anisotropy of foliated rocks with varied mica contents. Journal of Structural Geology 15, 1097–1121.
Simpson, C., 1985. Deformation of granitic rocks across the brittle–ductile transition. Journal of Structural Geology 7, 503–511.
Simpson, C., Schmid, S.M., 1983. An evaluation of criteria to determine the sense of movement in sheared rocks. Bulletin of the Geological Society of America 94, 1281–1288.
Stipp, M., Stünitz, H., Heilbronner, R., Schmid, S.M., 2002. The eastern Tonale fault zone: a 'natural laboratory' for crystal plastic deformation of quartz over a temperature range from 250 to 700 °C. Journal of Structural Geology 24, 1861–1884.
Stöckhert, B., Brix, M.R., Kleinschrodt, R., Hurford, A.J., Wirth, R., 1999. Thermochronometry and microstructures of quartz – a comparison with experimental flow laws and predictions on the temperature of the brittle–plastic transition. Journal of Structural Geology 21, 351–369.
Stünitz, H., Fitz Gerald, J.D., 1993. Deformation of granitoids at low metamorphic grade II: granular flow in albite-rich mylonites. Tectonophysics 221, 299–324.
Stünitz, H., Tullis, J., 2001. Weakening and strain localization produced by syn-deformational reaction of plagioclase. International Journal of Earth Sciences 90, 136–148.
Tourigny, G., Tremblay, A., 1997. Origin and incremental evolution of brittle/ductile shear zones in granitic rocks: natural examples from the southern Abitibi Belt, Canada. Journal of Structural Geology 19, 15–27.
Trepmann, C.A., Stöckhert, B., Dorner, D., Moghadam, R.H., Küster, M., Röller, K., 2007. Simulating coseismic deformation of quartz in the middle crust and fabric evolution during postseismic stress relaxation – an experimental study. Tectonophysics 442, 83–104.
Tullis, J., Wenk, H.R., 1994. Effect of muscovite on the strength and lattice preferred orientations of experimentally deformed quartz aggregates. Materials Science and Engineering A175, 209–220.
Van Daalen, M., Heilbronner, R., Kunze, K., 1999. Orientation analysis of localized shear deformation in quartz fibres at the brittle–ductile transition. Tectonophysics 303, 83–107.
Vernon, R.H., 2004. A Practical Guide to Rock Microstructure. Cambridge University Press, Cambridge.
Vernooij, M.G.C., Kunze, K., Den Brok, B., 2006a. 'Brittle' shear zones in experimentally deformed quartz single crystals. Journal of Structural Geology 28, 1292–1306.
Vernooij, M.G.C., Den Brok, B., Kunze, K., 2006b. Development of crystallographic preferred orientations by nucleation and growth of new grains in experimentally deformed quartz single crystals. Tectonophysics 427, 35–53.
Vollbrecht, A., Stipp, M., OlesenØ, N., 1999. Crystallographic orientation of microcracks in quartz and inferred deformation processes: a study on gneisses from the German Continental Deep Drilling Project (KTB). Tectonophysics 303, 279–297.
Wheleer, J., Prior, D.J., Jiang, Z., Spiess, R., Trimby, P.W., 2001. The petrological significance of misorientations between grains. Contributions to Mineralogy and Petrology 141, 109–124.